J. Fluid Mech. (2010), *vol.* 652, *pp.* 299–331.
doi:10.1017/S0022112009994125

On the boundary-layer structure of high-Prandtl-number horizontal convection

P. G. DANIELS†

Centre for Mathematical Science, City University, Northampton Square, London EC1V 0HB, UK

(Received 7 January 2009; revised 17 December 2009; accepted 17 December 2009)

This paper describes the boundary-layer structure of the steady flow of an infinite Prandtl number fluid in a two-dimensional rectangular cavity driven by differential heating of the upper surface. The lower surface and sidewalls of the cavity are thermally insulated and the upper surface is assumed to be either shear-free or rigid. In the limit of large Rayleigh number ($R \to \infty$), the solution involves a horizontal boundary layer at the upper surface of depth of order $R^{-1/5}$ where the main variation in the temperature field occurs. For a monotonic temperature distribution at the upper surface, fluid is driven to the colder end of the cavity where it descends within a narrow convection-dominated vertical layer before returning to the horizontal layer. A numerical solution of the horizontal boundary-layer problem is found for the case of a linear temperature distribution at the upper surface. At greater depths, of order $R^{-2/15}$ for a shear-free surface and order $R^{-9/65}$ for a rigid upper surface, a descending plume near the cold sidewall, together with a vertically stratified interior flow, allow the temperature to attain an approximately constant value throughout the remainder of the cavity. For a shear-free upper surface, this constant temperature is predicted to be of order $R^{-1/15}$ higher than the minimum temperature of the upper surface, whereas for a rigid upper surface it is predicted to be of order $R^{-2/65}$ higher.

1. Introduction

Many geophysical and industrial processes, such as heat transport in the oceans (Stern 1975) and furnace-melt flows in glass manufacture (Krause & Loch 2002), involve convection driven by horizontal thermal gradients at high Rayleigh number and moderate or high Prandtl number. This work is concerned with a formal asymptotic description of the steady infinite Prandtl number flow generated in a two-dimensional rectangular cavity by differential heating of the upper surface in the limit of large Rayleigh number, $R \to \infty$. The upper surface is shear-free or rigid and subject to a monotonic temperature differential, while the lower surface and sidewalls are rigid and thermally insulated.

Much work has been done to gain insight into the properties of such flows. Rossby (1965) conducted laboratory experiments for high Prandtl numbers up to 10^4 and Rayleigh numbers up to 10^{10} and argued that the heat flux and circulation scale as $R^{1/5}$ as $R \to \infty$, implying that major variations in the flow and temperature fields take place at depths of order $R^{-1/5}$ from the upper surface. This was supported by a numerical investigation for shear-free boundary conditions, Prandtl numbers

† Email address for correspondence: p.g.daniels@city.ac.uk

in the range 1–100 and Rayleigh numbers up to 10^8 by Rossby (1998). More recently, numerical simulations by Chiu-Webster, Hinch & Lister (2008) for an infinite Prandtl number fluid and Rayleigh numbers up to 10^{10} have confirmed the $R^{1/5}$ scaling for both rigid and shear-free upper surfaces. These authors also identify the main features of the asymptotic structure as $R \to \infty$, including the existence of a descending plume near the cold sidewall and a vertically stratified interior flow below the main horizontal boundary layer. At greater depths, within the core region of the cavity, variations in the temperature are of order R^{-1} and to a first approximation the temperature is constant. A similarity solution for the plume allows the transition between the stratified interior and the core to be described, and leads to results shown to be in excellent agreement with the numerical simulations.

A related horizontal boundary-layer/core structure involving an inverse decay of the streamfunction with depth arises in the equivalent porous medium problem (Daniels & Punpocha 2005) although there the scalings of the horizontal and vertical boundary layers are compatible and allow the main horizontal structure to match directly with the core region. In the present problem, the vertical boundary layer at depths of order $R^{-1/5}$ is convectively dominated and a full vertical-layer balance can only be achieved at slightly greater depths, giving rise to the plume and vertically stratified interior flow.

Other theoretical work on the high-Rayleigh-number limit includes that by Killworth & Manins (1980), who obtained a similarity solution of the horizontal boundary-layer equations for a quadratic temperature profile, and Hughes *et al.* (2007), who discussed a model based on a turbulent plume. Siggers, Kerswell & Balmforth (2004) derived a bound for the heat flux in the large Rayleigh number limit and obtained numerical results for shear-free boundary conditions for Rayleigh numbers up to 10^8 and Prandtl numbers up to 4. Numerical results have also been reported by Gramberg, Howell & Ockenden (2007) for an infinite Prandtl number fluid and Rayleigh numbers up to 7×10^8 and both they and Chiu-Webster *et al.* (2008) discuss asymptotic properties of the system for shallow geometries. Laboratory experiments with water at high Rayleigh numbers (up to 10^{10} and 10^{13} respectively) have been reported by Wang & Huang (2005) and Mullarney, Griffiths & Hughes (2004). Here the flow with a rigid upper surface is time dependent but the results provide support for the $R^{1/5}$ scaling, albeit in the unsteady regime.

Following a formulation of the problem in § 2, §§ 3–7 are concerned with the asymptotic structure of the solution as $R \to \infty$ for a shear-free upper surface. Section 3 provides an overview of the proposed structure and considers the main horizontal boundary-layer problem at depths of order $R^{-1/5}$ where a numerical solution is determined for the case of a linear temperature profile at the upper surface. Sinking motion is confined to the neighbourhood of the cold sidewall, consistent with the kind of behaviour of the oceanic circulation discussed by Stommel (1962) and is considered in §§ 4–6. The evolution of a descending plume governed by the vertical boundary-layer equations, together with a vertically stratified interior flow, is identified at depths of order $R^{-2/15}$. This is considered in § 7 and leads to an estimate of the leading-order contribution to the constant temperature in the underlying core region which, as $R \to \infty$, is predicted to be of order $R^{-1/15}$ higher than the minimum temperature of the upper surface. Modifications to the structure for the case of a rigid upper surface are considered in § 8 and the results are discussed and compared with the numerical computations of Chiu-Webster *et al.* (2008) in § 9.

2. Formulation

A rectangular two-dimensional cavity $0 \leqslant x^* \leqslant d, 0 \leqslant z^* \leqslant h$ is filled with an infinite Prandtl number fluid. The upper surface $z^* = h$ is held at temperature

$$T^* = T_0^* + \Delta T\, S(x^*/d), \tag{2.1}$$

where the function $S(x^*/d)$ varies monotonically from zero at $x^* = 0$ to 1 at $x^* = d$. The vertical walls $x^* = 0$ and $x^* = d$ and the bottom wall $z^* = 0$ are rigid and thermally insulated whilst the upper surface is assumed to be either shear-free or rigid. Subject to the Oberbeck–Boussinesq approximation, steady two-dimensional motion is governed by the non-dimensional vorticity and heat conservation equations

$$\nabla^4 \psi = R \frac{\partial T}{\partial x}, \tag{2.2}$$

$$\nabla^2 T = \frac{\partial \psi}{\partial x}\frac{\partial T}{\partial z} - \frac{\partial \psi}{\partial z}\frac{\partial T}{\partial x}, \tag{2.3}$$

where T is the temperature measured relative to T_0^* and non-dimensionalized by ΔT, ψ is the streamfunction non-dimensionalized by the thermal diffusivity κ, $(x, z) = (x^*/d, (h - z^*)/d)$ are non-dimensional Cartesian coordinates with the origin at the upper cold corner and the z axis vertically downwards, and R is the Rayleigh number defined by

$$R = \frac{\beta g \Delta T d^3}{\nu \kappa}, \tag{2.4}$$

where β is the coefficient of thermal expansion, g is the acceleration due to gravity and ν is the kinematic viscosity. The non-dimensional velocity components in the x, z directions are given by

$$u = -\frac{\partial \psi}{\partial z}, \quad w = \frac{\partial \psi}{\partial x}, \tag{2.5}$$

respectively.

The boundary conditions at the vertical sidewalls are

$$\psi = \frac{\partial \psi}{\partial x} = \frac{\partial T}{\partial x} = 0 \text{ on } x = 0, 1 \tag{2.6}$$

and at the lower surface

$$\psi = \frac{\partial \psi}{\partial z} = \frac{\partial T}{\partial z} = 0 \text{ on } z = A, \tag{2.7}$$

where $A = h/d$ is the aspect ratio of the cavity. If the upper surface is shear-free then

$$\psi = \frac{\partial^2 \psi}{\partial z^2} = 0, \quad T = S(x) \text{ on } z = 0, \tag{2.8}$$

while if it is a rigid boundary then

$$\psi = \frac{\partial \psi}{\partial z} = 0, \quad T = S(x) \text{ on } z = 0. \tag{2.9}$$

Note that it follows from (2.3), (2.6) and (2.7) that the total heat transfer through the upper surface is zero,

$$\int_0^1 \frac{\partial T}{\partial z}(x, 0)\mathrm{d}x = 0, \tag{2.10}$$

but a Nusselt number can be defined by summing the inward and outward contributions, giving

$$Nu = \int_0^1 \left| \frac{\partial T}{\partial z}(x, 0) \right| \mathrm{d}x. \tag{2.11}$$

Solutions of the problem (2.2), (2.3), (2.6), (2.7) and either (2.8) or (2.9) depend not only on the Rayleigh number R and aspect ratio A but also on the specific form of the temperature profile $S(x)$. Numerical solutions reported recently by Gramberg *et al.* (2007) and Chiu-Webster *et al.* (2008) cover a wide range of values of R and A and linear and quadratic temperature profiles S. These indicate that the temperature differential at the upper surface drives a circulation whose centre moves towards the upper cold corner of the cavity as R increases. This paper is concerned with a description of the asymptotic structure of the solution as $R \to \infty$ for finite values of A and general monotonic temperature profiles S with finite gradient. Detailed calculations are carried out for the linear profile $S = x$.

3. Shear-free upper surface

A schematic diagram of the main regions of the proposed asymptotic structure as $R \to \infty$ for a shear-free upper surface is shown in figure 1. The thermal gradient along the upper surface drives fluid to the cold end of the cavity within a horizontal boundary layer of depth $R^{-1/5}$ (region I) where the streamfunction is of order $R^{1/5}$. At the hot end of the layer, there is an upward motion which is reduced to rest within a passive wall layer of thickness $R^{-3/10}$ (region II). Fluid driven to the cold end of the horizontal boundary layer enters a convectively dominated vertical boundary layer of width $R^{-4/15}$ (region III), where it descends and returns to the horizontal layer, completing the main order $R^{1/5}$ circulation within the cavity. The vertical layer problem is considered in § 4, and an analysis of the solution as the centre of circulation is approached reveals an intricate structure in which the streamfunction rises above its value in the horizontal boundary layer, reaching a maximum of order $R^{11/45}$ within a vortex region (region IV) studied in § 5. Here the flow consists of closed streamlines and is isothermal by analogy with the Prandtl–Batchelor theorem (Batchelor 1954, 1956). Between the vertical boundary layer and the cold sidewall there is a thermal adjustment within an inner vertical layer (region V). This is studied in § 6 and an analytical solution allows the leading-order wall temperature, which increases with depth, to be determined. This solution also reveals a breakdown of the double vertical layer structure at depths of order $R^{-2/15}$ and the evolution of a descending plume (region VI) together with a vertically stratified interior flow in an outer horizontal layer (region VII). Fluid is detrained from the plume into this outer layer where it rises and returns to the main horizontal boundary layer, completing the circulation of fluid for which the streamfunction is of order $R^{2/15}$. The upflow generated at the hot end of the outer horizontal layer is reduced to rest within a passive wall layer (region VIII) of thickness $R^{-4/15}$. The temperature variation in regions VI, VII and VIII is of order $R^{-1/15}$, and as the underlying core region is approached it saturates at a constant value which is determined approximately in § 7. The core region (region IX) contains the weakest part of the circulation, with temperature variations of order R^{-1} and order one values of the streamfunction governed by the full equations of motion.

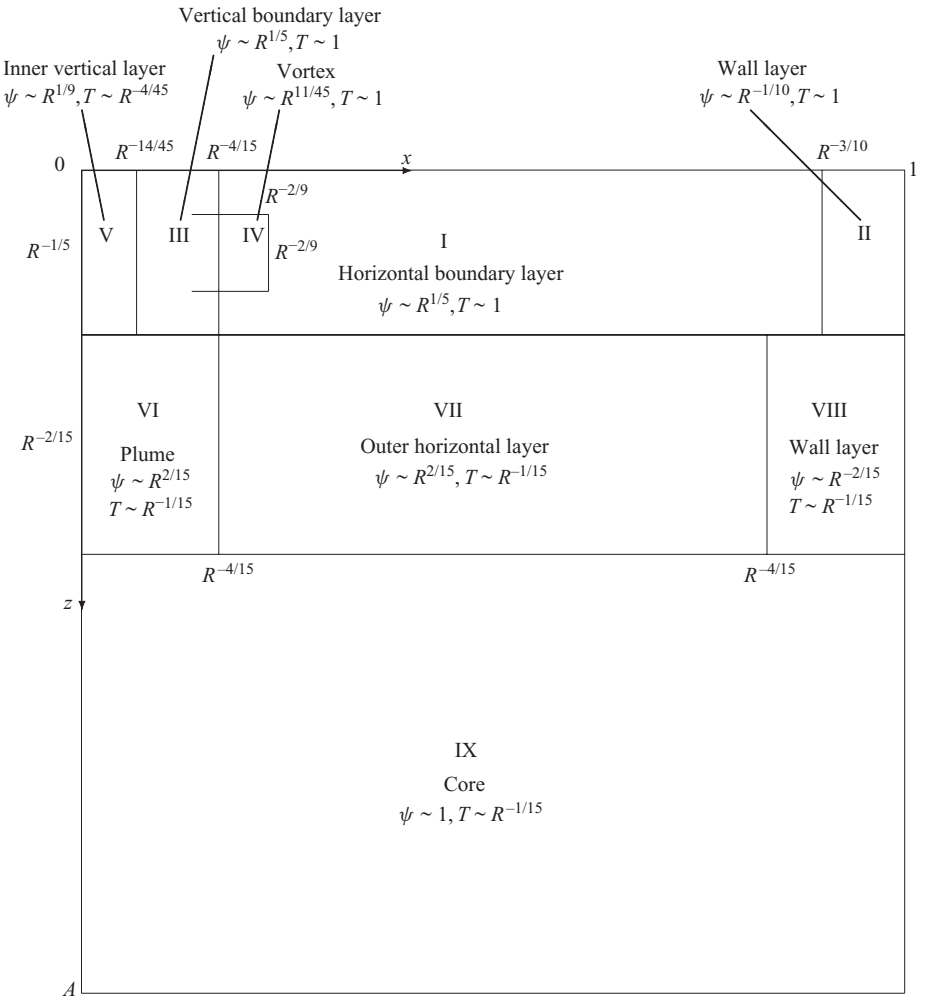

FIGURE 1. Schematic diagram of the main regions of the asymptotic structure of the solution for a shear-free upper surface in the limit $R \to \infty$. The leading-order scalings of ψ and T in each region are shown.

3.1. *Horizontal boundary layer*

In the main horizontal boundary layer (region I), a balance between friction and buoyancy in the vorticity equation and conduction and convection in the heat equation requires that

$$\psi = R^{1/5}\Psi(x, Z) + \cdots, \quad T = \Theta(x, Z) + \cdots, \quad R \to \infty, \tag{3.1}$$

where $z = R^{-1/5}Z$. Substitution into (2.2) and (2.3) shows that Ψ and Θ satisfy the equations

$$\frac{\partial \Theta}{\partial x} - \frac{\partial^4 \Psi}{\partial Z^4} = 0, \quad \frac{\partial^2 \Theta}{\partial Z^2} - \frac{\partial \Psi}{\partial x}\frac{\partial \Theta}{\partial Z} + \frac{\partial \Psi}{\partial Z}\frac{\partial \Theta}{\partial x} = 0. \tag{3.2}$$

These must be solved subject to

$$\Psi = \frac{\partial^2 \Psi}{\partial Z^2} = 0, \quad \Theta = S(x) \text{ on } Z = 0, \tag{3.3}$$

$$\Psi = \frac{\partial \Theta}{\partial x} = 0 \text{ on } x = 1, \tag{3.4}$$

$$\Theta = F(\Psi) \text{ on } x = 0 \tag{3.5}$$

and

$$\Psi \to 0 \text{ as } Z \to \infty. \tag{3.6}$$

Here (3.3) are the conditions on the shear-free upper surface. The conditions (3.4) at the hot end ensure a consistent match with the wall layer (region II in figure 1) where the vertical component of velocity is reduced to zero. Here the flow takes place within the stably stratified thermal field generated at the end of the horizontal boundary layer. A balance between friction and buoyancy in the vorticity equation and conduction and convection in the heat equation requires that

$$\psi = R^{-1/10}\tilde{\Psi}(\bar{x}, Z) + \cdots, \quad T = \Theta(1, Z) + R^{-1/5}\tilde{\Theta}(\bar{x}, Z) + \cdots, \quad R \to \infty, \tag{3.7}$$

where $x = 1 - R^{-3/10}\bar{x}$ and $\tilde{\Psi}, \tilde{\Theta}$ satisfy the equations

$$\frac{\partial^4 \tilde{\Psi}}{\partial \bar{x}^4} = -\frac{\partial \tilde{\Theta}}{\partial \bar{x}}, \quad \frac{\partial \tilde{\Theta}}{\partial \bar{x}^2} - \frac{\mathrm{d}\lambda}{\mathrm{d}Z} = \lambda \frac{\partial \tilde{\Psi}}{\partial \bar{x}}, \tag{3.8}$$

with $\lambda = -\mathrm{d}\Theta(1, Z)/\mathrm{d}Z > 0$ to be determined by the horizontal boundary-layer solution. The wall conditions are

$$\tilde{\Psi} = \frac{\partial \tilde{\Psi}}{\partial \bar{x}} = \frac{\partial \tilde{\Theta}}{\partial \bar{x}} = 0 \text{ on } \bar{x} = 0, \tag{3.9}$$

and matching with the horizontal boundary layer requires

$$\tilde{\Psi} \sim -\bar{x}\lambda^{-1}\frac{\mathrm{d}\lambda}{\mathrm{d}Z} \text{ as } \bar{x} \to \infty. \tag{3.10}$$

The required solution is

$$\tilde{\Psi} = \lambda^{-1}\frac{\mathrm{d}\lambda}{\mathrm{d}Z}\left\{-\bar{x} + \sqrt{2}\lambda^{-1/4}\mathrm{e}^{-\lambda^{1/4}\bar{x}/\sqrt{2}}\sin(\lambda^{1/4}\bar{x}/\sqrt{2})\right\}. \tag{3.11}$$

At the cold end of the horizontal boundary layer, fluid enters the vertical boundary layer (region III in figure 1), where it descends and returns to the horizontal layer. Condition (3.5) expresses the fact that the vertical layer is convectively dominated (see § 4), with the functional relation F between Θ and Ψ to be determined by the solution in the horizontal layer. The final condition (3.6) specifies that the horizontal layer encompasses the main return flow across the cavity, so that the order $R^{1/5}$ circulation is completed within these horizontal and vertical layers.

It can be expected from (3.2) and (3.3) that in region I at $x = 0$,

$$\Psi = a_1 Z + a_3 Z^3 + \cdots, \quad \Theta = b_1 Z + b_2 Z^2 + \cdots \text{ as } Z \to 0, \tag{3.12}$$

implying that

$$F(\Psi) = K\Psi + L\Psi^2 + \cdots \text{ as } \Psi \to 0, \tag{3.13}$$

where $K = b_1/a_1 > 0$ and $L = b_2/a_1^2$. It follows from the vorticity equation in (3.2) that Θ must become independent of x as $Z \to \infty$. The heat equation then requires that $\partial\Psi/\partial x$ becomes independent of x and, together with (3.13), that both Ψ and Θ are inversely proportional to Z as $Z \to \infty$. Making use of (3.4) leads to the asymptotic forms

$$\Psi = \frac{2(1-x)}{Z} + \frac{8L(1-x)\ln Z}{3KZ^2} + O(Z^{-2}), \quad \Theta = \frac{2K}{Z} + \frac{8L\ln Z}{3Z^2} + O(Z^{-2}), \tag{3.14}$$

as $Z \to \infty$ for $0 \leqslant x \leqslant 1$. Here the logarithmic terms are generated if L is non-zero because the correction terms generated by L in (3.13) would otherwise resonate with the existence of an arbitrary origin shift in Z which arises in the order Z^{-2} corrections in (3.14). Equivalently, this shift D can be combined directly with Z to give the asymptotic form

$$\Psi \sim \frac{1-x}{Z+D}\left\{2+\frac{8L\ln(Z+D)}{3K(Z+D)}\right\}, \quad Z \to \infty, \tag{3.15}$$

correct to order $(Z+D)^{-2}$. One of the main implications of (3.13) and (3.14) is that the temperature does not contain a finite non-zero contribution as $Z \to \infty$.

The horizontal boundary-layer problem was solved numerically using an explicit finite-difference scheme. Artificial time derivatives $\partial\Psi/\partial t$ and $\partial\Theta/\partial t$ are inserted on the right-hand sides of the vorticity and heat conservation equations (3.2), allowing the solution to be computed forwards in time until a steady state is achieved. The equations are discretized at all internal grid points using forward differences with step length Δt for the time derivatives and central differences with step lengths Δx and ΔZ for the spatial derivatives. Along the upper surface the boundary conditions (3.3) supply the values of Θ and Ψ, and the condition on $\partial^2\Psi/\partial Z^2$ allows the external values of Ψ needed in the five-point discretization of $\partial^4\Psi/\partial Z^4$ to be expressed in terms of internal values. At the hot end, the values of Ψ and Θ are determined from (3.4) using a quadratic interpolation based on two internal grid points in the case of Θ. At the cold end, values of Ψ on $x = 0$ are provided by a simple linear extrapolation based on two internal grid points. The same is done for Θ in $Z < Z_M$, where Z_M is the grid point at which the value of Ψ is greatest on $x = 0$. For $Z > Z_M$, the condition (3.5) is applied by specifying Θ as the value corresponding to that at the same value of Ψ in $Z < Z_M$. This is achieved by using a quadratic fit based on three neighbouring grid points on $x = 0$ surrounding the relevant value of Ψ in $Z < Z_M$. At the outer edge of the layer, taken numerically at $Z = Z_\infty$, the final condition (3.6) is applied by specifying Ψ from formula (3.15) with values of K and L obtained by fitting formula (3.13) at the grid points $Z = \Delta Z$ and $2\Delta Z$ on $x = 0$. Formula (3.15) is used to specify Ψ on $Z = Z_\infty$ and $Z = Z_\infty + \Delta Z$ for $0 \leqslant x \leqslant 1$, and Θ is specified at the same locations by its value at $x = 0$. In (3.15), the value of the origin shift D is updated by calculating it from the value of Ψ at $x = 0$, $Z = Z_\infty - \Delta Z$.

The scheme was started at $t = 0$ from an initial state

$$\Psi = \frac{2Z(1-x)}{1+Z^2}, \quad \Theta = S(x)\mathrm{e}^{-Z} + \frac{2KZ}{1+Z^2}, \tag{3.16}$$

with K in the range of 0.3–0.7. Other initial states were also tested to ensure that the solution converged to the same steady state. Detailed calculations were carried out for the linear temperature profile

$$S(x) = x \tag{3.17}$$

for a range of different step sizes Δx, ΔZ and outer boundaries Z_∞. For $\Delta x = 0.05$ and $\Delta Z = 0.2$, numerical stability was found to be maintained with a time step of $\Delta t = 0.0001$ or less, and convergence to a steady state was achieved typically to six significant figures in D at $t_\infty = 600$, although values of K, L and the temperature and streamfunction fields converged to the same level of accuracy significantly faster, at around $t_\infty = 400$. The most accurate computations with $\Delta x = 0.025$, $\Delta Z = 0.2$, $Z_\infty = 20$ and $\Delta t = 0.00004$ gave a steady-state solution with

$$K = 0.728, \quad L = -0.627, \quad D = -0.938 \tag{3.18}$$

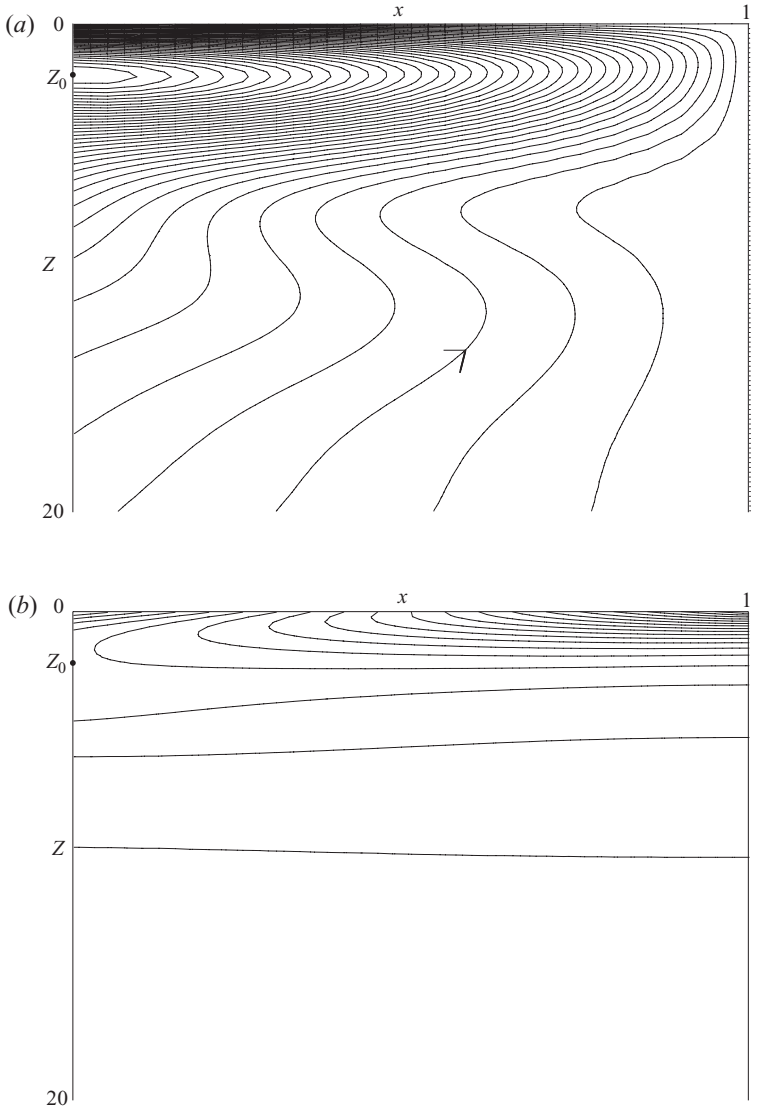

FIGURE 2. Streamlines (a) and isotherms (b) of the horizontal boundary-layer solution for a shear-free upper surface with a linear temperature profile. Intervals in Ψ and Θ are 0.02 and 0.05, respectively. The point $Z_0 = 2.10$ is shown.

and maximum values of Ψ and Θ on $x = 0$ given by

$$\Psi = \Psi_0 = 0.736, \quad \Theta = \Theta_0 = 0.244 \text{ at } Z = Z_0 = 2.10. \tag{3.19}$$

In the above results, the value of D is the most difficult to obtain accurately, being associated with the third term in the asymptotic form of Ψ at large Z. Figure 2 shows the streamlines and isotherms of the horizontal boundary-layer flow, and the profiles of Ψ and Θ at $x = 0$ are shown in figure 3 along with the functional relation $\Theta = F(\Psi)$. In the neighbourhood of Z_0

$$\Psi(0, Z) = \Psi_0 - \Psi_1(Z - Z_0)^2 + \cdots, \quad \Theta(0, Z) = \Theta_0 - \Theta_1(Z - Z_0)^4 + \cdots, \tag{3.20}$$

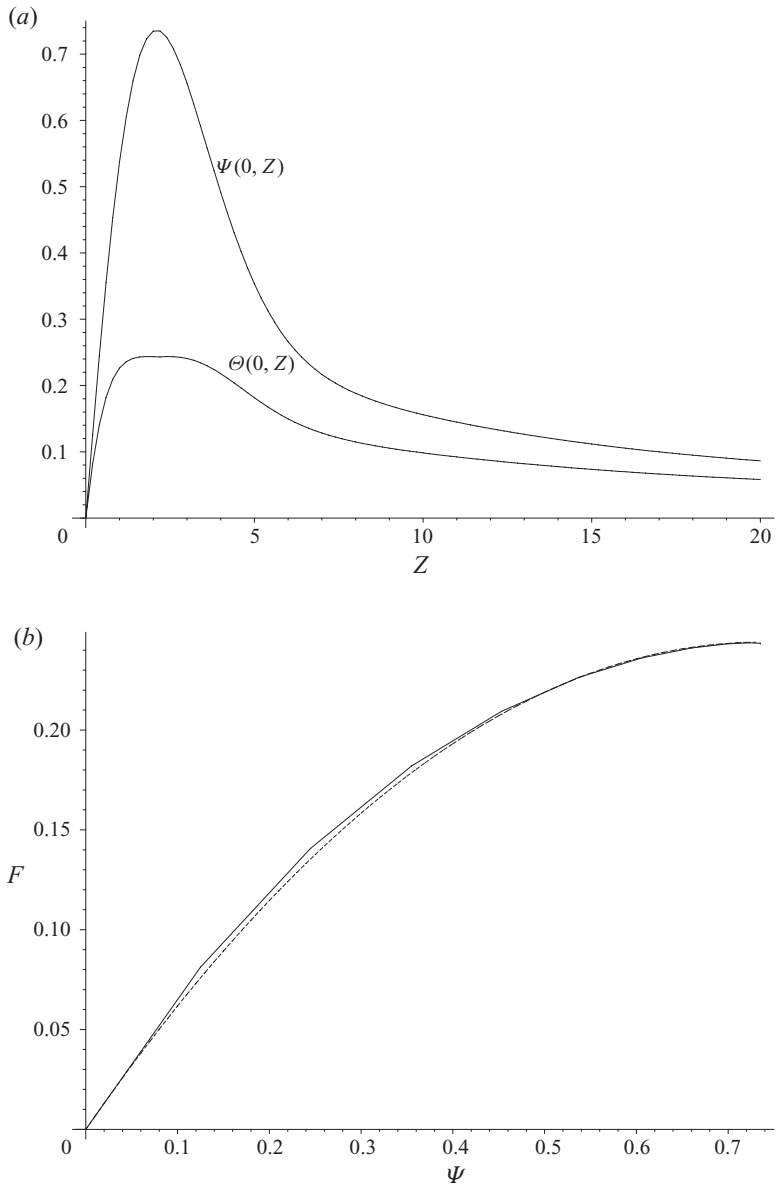

FIGURE 3. Horizontal boundary-layer solution for a shear-free upper surface with a linear temperature profile showing (*a*) the profiles $\Psi(0, Z)$ and $\Theta(0, Z)$ and (*b*) the function $F(\Psi)$ along with an analytical approximation given in (4.6) (- - -).

with the values of Ψ_1 and Θ_1 estimated to be

$$\Psi_1 = 0.132, \quad \Theta_1 = 0.0087, \tag{3.21}$$

and it follows that the gradient of F reaches zero at $\Psi = \Psi_0$. The plateau form of the temperature associated with (3.20) and evident in figure 3 results from the fact that since the maxima of $\Psi(0, Z)$ and $\Theta(0, Z)$ must coincide at $Z = Z_0$, the convective terms in the heat conservation equation (3.2) vanish there, and to avoid a local singularity $\partial^2\Theta/\partial Z^2$ must also vanish there. Thus, Θ cannot be locally quadratic in

$Z - Z_0$, and instead has a quartic form. From (3.2), the dominant terms in the Taylor expansion of $\Theta(x, Z)$ about $x = 0, Z = Z_0$ are expected to be

$$\Theta \sim \Theta_0 + \delta x^2 - 6\Theta_1 \Psi_1^{-1} x(Z - Z_0) - \Theta_1 (Z - Z_0)^4, \tag{3.22}$$

where $2\delta = \partial^2 \Theta / \partial x^2(0, Z_0)$, so that as $x \to 0, Z \to Z_0$ the isotherms $\Theta = \Theta_0$ approach along the paths $x \sim \Psi_1 (Z_0 - Z)^3/6$ and $x \sim 6\Theta_1 (\Psi_1 \delta)^{-1} (Z - Z_0)$ with the vertices of the isotherms (see figure 2*b*) located at $x \sim 2\Psi_1 (Z_0 - Z)^3/3$. Formula (3.22) is consistent with the upward slope of the isotherms from $x = 0$ either side of $Z = Z_0$ in figure 2(*b*).

It should be added that for the linear temperature profile (3.17), the condition (3.4) implies a weak singularity of the horizontal boundary-layer solution at $x = 1, Z = 0$. The change in horizontal thermal gradient at the corner leads to a region where $Z \sim (1-x)^{1/3}$, $\Psi \sim (1-x)^{4/3}$ and $\Theta = 1 - O((1-x)^{1/3})$, and it is anticipated that use of a uniform numerical grid in x and Z results in only minor loss of accuracy away from the corner.

The horizontal boundary-layer solution determines the leading-order contribution to the Nusselt number $Nu \sim R^{1/5} Nu_0$ as $R \to \infty$, where

$$Nu_0 = \int_0^1 \left| \frac{\partial \Theta}{\partial Z}(x, 0) \right| \mathrm{d}x. \tag{3.23}$$

The numerical results gave $Nu_0 = 0.27$.

4. Vertical boundary layer

The vertical layer that conveys fluid from and then back to the horizontal layer at the cold end (region III in figure 1) is convectively dominated, with the functional relation between streamfunction and temperature determined by the horizontal layer. Thus,

$$\psi = R^{1/5} \bar{\Psi}(\bar{X}, Z) + \cdots, \quad T = \bar{\Theta}(\bar{X}, Z) + \cdots, \quad R \to \infty, \tag{4.1}$$

where $x = R^{-4/15} \bar{X}$, $\bar{\Theta} = F(\bar{\Psi})$ and $\bar{\Psi}$ satisfies the equation

$$\frac{\partial^3 \bar{\Psi}}{\partial \bar{X}^3} = F(\bar{\Psi}) - F(\bar{\Psi}_\infty), \tag{4.2}$$

with boundary conditions

$$\bar{\Psi} = \frac{\partial \bar{\Psi}}{\partial \bar{X}} = 0 \text{ on } \bar{X} = 0 \tag{4.3}$$

and

$$\bar{\Psi} \to \bar{\Psi}_\infty = \Psi(0, Z) \text{ as } \bar{X} \to \infty. \tag{4.4}$$

Here the magnitudes of ψ and T in (4.1) are set by matching with the horizontal boundary layer and the scaling of x is determined by the need for friction to balance buoyancy in (4.2). This has the consequence that the conduction terms in the heat equation are smaller than the convection terms by a factor of $R^{-2/15}$. The horizontal boundary-layer profiles $\psi \sim R^{1/5} \Psi(0, Z)$ and $T \sim \Theta(0, Z)$ cannot change on a longer scale $x \sim R^{-1/5}$ comparable with the boundary-layer depth because the governing equations (2.2) and (2.3) are then dominated by buoyancy and convection, implying that to a first approximation T and ψ are independent of the horizontal coordinate.

Since $F'(\bar{\Psi}_\infty) > 0$ for $0 \leqslant \bar{\Psi}_\infty < \Psi_0$ (see figure 3), (4.2) admits two solutions $\bar{\Psi}$ that decay as $\bar{X} \to \infty$, allowing the two wall conditions (4.3) to be satisfied. Although the

conditions (4.3) imply that $\partial\bar{\Theta}/\partial\bar{X} = 0$ at $\bar{X} = 0$, there is a further adjustment to the temperature within an inner vertical layer to be considered in § 6.

The vertical coordinate Z enters the system (4.2)–(4.4) only indirectly through $\bar{\Psi}_\infty$. For each value of $\bar{\Psi}_\infty$ such that $0 < \bar{\Psi}_\infty < \Psi_0$, the solution is applicable at two values of Z, one each side of Z_0.

The solution of the vertical boundary-layer problem (4.2)–(4.4) can be found analytically for small and large values of Z because $F(\bar{\Psi}) \sim K\bar{\Psi}$ as $\bar{\Psi} \to 0$, and so (4.2) becomes linear. The required solution as $\bar{\Psi}_\infty \to 0$ is

$$\bar{\Psi} \sim \bar{\Psi}_\infty f(K^{1/3}\bar{X}), \quad f(\bar{X}) = 1 - \mathrm{e}^{-\bar{X}/2}\left\{\cos(\sqrt{3}\bar{X}/2) + \frac{1}{\sqrt{3}}\sin(\sqrt{3}\bar{X}/2)\right\}, \tag{4.5}$$

where, from (3.12) and (3.14), $\bar{\Psi}_\infty \sim a_1 Z$, $Z \to 0$ and $\bar{\Psi}_\infty \sim 2Z^{-1}$, $Z \to \infty$. Although modifications to the vertical boundary-layer solution might be anticipated at depths of order $R^{-4/15}$ near the upper surface where the full form of the vorticity equation (2.2) comes into play, the z derivatives in the biharmonic operator do not affect the leading contribution to (4.5) as $Z \to 0$, which therefore remains a uniformly valid first approximation to the solution near the upper surface.

For general values of Z, rather than using the numerically generated function F in (4.2), which would lead to a substantial numerical task, it is useful to approximate F by an analytical formula. A suitable approximation (see figure 3) is

$$F(\bar{\Psi}) = \frac{\Theta_0\bar{\Psi}(2\Psi_0 - \bar{\Psi})}{\Psi_0^2}, \quad 0 \leqslant \bar{\Psi} \leqslant \Psi_0. \tag{4.6}$$

Since solutions $\bar{\Psi}$ of (4.2) approach $\bar{\Psi}_\infty$ with oscillatory decay, it is anticipated that at certain locations within the vertical boundary layer $\bar{\Psi}$ will exceed Ψ_0. In that case, the vertical layer, together with the vortex region to be discussed in § 5, is a convectively dominated region containing closed streamlines bounded by $\bar{\Psi} = \Psi_0$. By reference to the thermal equivalent of the Prandtl–Batchelor theorem (see Gramberg *et al.* 2007), it is therefore assumed that

$$F(\bar{\Psi}) = \Theta_0, \quad \bar{\Psi} > \Psi_0. \tag{4.7}$$

The vertical boundary-layer problem (4.2)–(4.7) is now simplified through the scalings

$$\bar{\Psi} = \Psi_0\phi(X, Z), \quad \bar{\Psi}_\infty = \Psi_0\phi_\infty(Z), \quad \bar{X} = (\Psi_0/\Theta_0)^{1/3}X \tag{4.8}$$

to give the system

$$\frac{\partial^3\phi}{\partial X^3} + (1-\phi)^2 = (1-\phi_\infty)^2, \quad \phi < 1, \tag{4.9}$$

$$\frac{\partial^3\phi}{\partial X^3} = (1-\phi_\infty)^2, \quad \phi > 1, \tag{4.10}$$

with

$$\phi = \frac{\partial\phi}{\partial X} = 0 \text{ on } X = 0, \tag{4.11}$$

$$\phi \to \phi_\infty \text{ as } X \to \infty, \tag{4.12}$$

to be solved for $0 < \phi_\infty < 1$. Solutions were found using a fourth-order Runge–Kutta scheme. For values of ϕ_∞ from 0 to 0.85, this was done by computing inwards from

the asymptotic form

$$\phi \sim \phi_\infty + \mathrm{e}^{-\omega_\infty X/2}\left\{A\cos(\sqrt{3}\omega_\infty X/2) + B\sin(\sqrt{3}\omega_\infty X/2)\right\}, \quad X \to \infty, \tag{4.13}$$

where $\omega_\infty = 2^{1/3}(1-\phi_\infty)^{1/3}$, starting from an outer boundary $X = X_\infty$. Values of the constants A and B were adjusted by Newton iteration to achieve convergence of the solution to the boundary conditions (4.11) at a given value of ϕ_∞ and then these values were used as initial guesses for the next value of ϕ_∞. The whole solution was started from small values of ϕ_∞, where (4.13) is equivalent to (4.5) and is valid for the whole range $0 \leqslant X < \infty$ with $A = \sqrt{3}B = -\phi_\infty$ and $\omega_\infty = 2^{1/3}$ to a first approximation. Profiles of ϕ for various values of ϕ_∞ up to 0.85 obtained with a step in X of 0.01 and an outer boundary $X_\infty = 10$ are shown in figure 4(a). Tests were made with other step sizes and outer boundaries to check the accuracy of the results. For $\phi_\infty > 0.77$ the value of ϕ exceeds 1 in part of the domain and thus (4.10) comes into play. For ϕ_∞ greater than 0.85, the growth in ϕ was such that the method of inward computation from (4.13) no longer worked effectively and an alternative approach had to be adopted. Results for $0.85 \leqslant \phi_\infty < 1$ were obtained instead by computing outwards from the conditions (4.11), choosing the value of $\alpha = \partial^2\phi/\partial X^2(X=0)$ to ensure that $\phi \to \phi_\infty$ as $X \to \infty$. In practice, if α is too large the solution continues to increase, with (4.10) applicable at large X, or if α is too small the solution decreases into a singularity. By gradually increasing the outer limit of the computation, the required solution can be found. Figure 4(b) shows the profiles of ϕ obtained in this way for $\phi_\infty = 0.85, 0.9$ and 0.95.

As ϕ_∞ approaches 1, an ever larger region in X emerges in which ϕ exceeds 1, and the maximum value of ϕ over the domain $0 \leqslant X < \infty$ increases without bound. Figure 5(a) shows ϕ_{max}, the maximum value of ϕ over the domain $0 \leqslant X < \infty$, as a function of ϕ_∞, and also the corresponding variation of α, which remains finite as $\phi_\infty \to 1$. Figure 5(b) shows the position, X_{max}, at which $\phi = \phi_{max}$ as a function of ϕ_∞, along with the boundary of the region in which $\phi > 1$. The outer section of this boundary increases without bound as $\phi_\infty \to 1$, while the inner section approaches a finite value of X. This region in which the temperature is constant and equal to Θ_0 is the outer part of a vortex centred on Z_0, which is considered in detail in § 5. In order to ascertain the structure of the vortex, it is helpful to investigate the limiting form of the vertical boundary-layer solution as $Z \to Z_0$ (that is, as $\phi_\infty \to 1$) in more detail, as follows.

4.1. *Asymptotic structure of the vertical boundary layer as* $Z \to Z_0$

This can be analysed by introducing a small parameter $\epsilon = 1 - \phi_\infty$ and considering the limiting form of the system (4.9)–(4.12) as $\epsilon \to 0$. Replacing ϕ_∞ in terms of ϵ, the system has the form

$$\frac{\partial^3\phi}{\partial X^3} + (1-\phi)^2 = \epsilon^2, \quad \phi < 1, \tag{4.14}$$

$$\frac{\partial^3\phi}{\partial X^3} = \epsilon^2, \quad \phi > 1, \tag{4.15}$$

$$\phi = \frac{\partial\phi}{\partial X} = 0 \text{ on } X = 0, \tag{4.16}$$

$$\phi \to 1 - \epsilon \text{ as } X \to \infty. \tag{4.17}$$

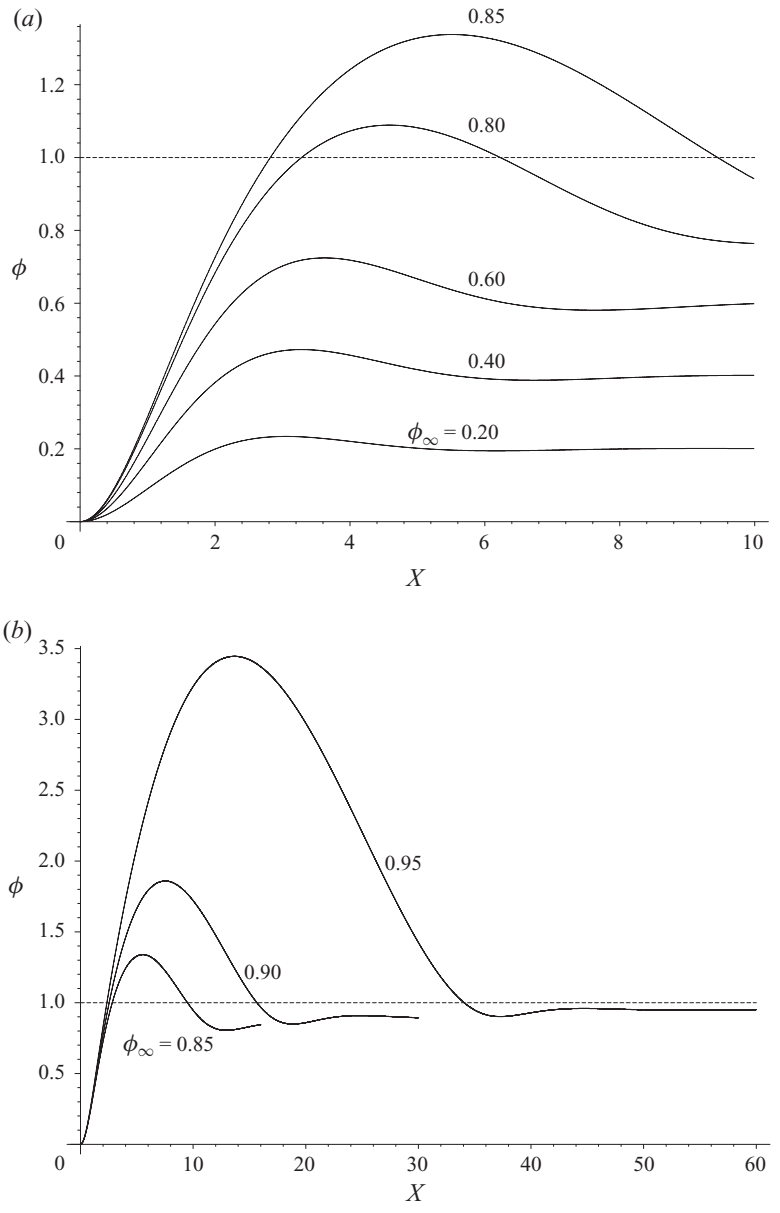

FIGURE 4. Profiles $\phi(X)$ in the vertical boundary layer at (*a*) $\phi_\infty = 0.20, 0.40, 0.60, 0.80, 0.85$ and (*b*) $\phi_\infty = 0.85, 0.90$ and 0.95 for a shear-free upper surface with a linear temperature profile. Sections of the curves above the dashed line correspond to isothermal flow.

Adjacent to the origin there is an inner region where $0 \leqslant X \leqslant X_0$ and ϕ increases from 0 to 1, where to a first approximation $\phi = \tilde{\phi}(X) + \cdots$ as $\epsilon \to 0$ and

$$\tilde{\phi}''' + (1 - \tilde{\phi})^2 = 0; \quad \tilde{\phi} = \tilde{\phi}' = 0 \text{ on } X = 0, \quad \tilde{\phi} = 1, \tilde{\phi}'' = 0 \text{ on } X = X_0. \tag{4.18}$$

Here the condition on $\tilde{\phi}''$ at $X = X_0$ is needed to ensure that $\phi = o(\epsilon^{-2})$ in the vortex region where $X - X_0 = O(\epsilon^{-1})$, to be discussed next. A numerical solution of (4.18)

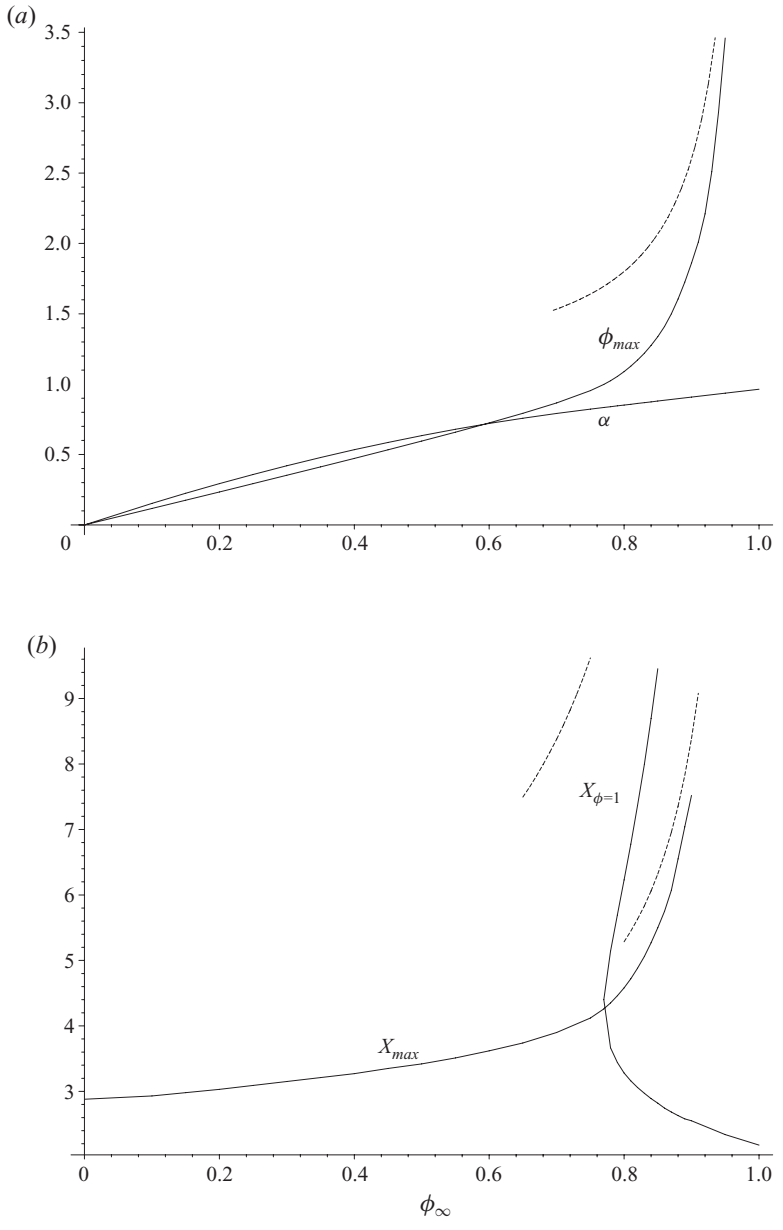

FIGURE 5. Properties of the vertical boundary-layer solution as a function of ϕ_∞ for a shear-free upper surface with a linear temperature profile showing (a) the maximum streamfunction ϕ_{max} along with the asymptotic form (4.31) as $\phi_\infty \to 1$ (- - -), and the scaled wall shear $\alpha = \partial^2\phi/\partial X^2(X = 0)$ and (b) the position X_{max} of the maximum streamfunction and the vortex boundary $X_{\phi=1}$ along with the asymptotic forms (4.32) and (4.33) as $\phi_\infty \to 1$ (- - -).

gives

$$X_0 = 2.18, \qquad \tilde{\phi}'(X_0) = \beta_0 = 0.579, \qquad \tilde{\phi}''(0) = \alpha_0 = 0.964. \tag{4.19}$$

The value of α_0 is the limiting value of $\partial^2\phi/\partial X^2(X = 0)$ as $\phi_\infty \to 1$ in figure 5(a) and the value of X_0 is the inner limiting boundary value of X as $\phi_\infty \to 1$ in figure 5(b).

The vertical flow β_0 at $X = X_0$ generates the main vortex in an outer region where $X - X_0 = O(\epsilon^{-1})$, and it emerges that the asymptotic structure of the solution has a remarkable form consisting of a series of inner and outer regions as $\epsilon \to 0$, with the inner regions governed by (4.14) and the outer regions governed by (4.15). In order to treat each of these regions concurrently, it is convenient to consider an outer region generated by a vertical flow

$$\frac{\partial \phi}{\partial X} = \epsilon^m \beta_m \text{ at } X = X_m, \tag{4.20}$$

so that the main vortex corresponds to the case where the index $m = 0$. The outer solution is given by

$$\phi - 1 = \epsilon^{(3m-2)/2} \phi_m(\xi_m) + \cdots, \quad \epsilon \to 0, \tag{4.21}$$

where $X = X_m + \epsilon^{(m-2)/2}\xi_m$ and $\phi_m > 0$ so that ϕ_m satisfies the system

$$\phi_m''' = 1; \quad \phi_m = 0, \phi_m' = \beta_m \text{ on } \xi_m = 0, \quad \phi_m = 0, \phi_m' = 0 \text{ on } \xi_m = \gamma_m. \tag{4.22}$$

Here the conditions at the unknown outer boundary $\xi_m = \gamma_m$ are needed in order to match with the solution in the next inner region. The solution of (4.22) is

$$\phi_m = \beta_m \xi_m - \left(\frac{2\beta_m}{3}\right)^{1/2} \xi_m^2 + \frac{1}{6}\xi_m^3, \quad 0 < \xi_m < \gamma_m, \tag{4.23}$$

where $\gamma_m = (6\beta_m)^{1/2}$. The maximum value of ϕ_m is $2(6\beta_m)^{3/2}/81$ at $\xi_m = (6\beta_m)^{1/2}/3$.

The next inner region is generated by the non-zero second derivative of ϕ_m at $\xi_m = \gamma_m$, and occupies the region $0 < \tilde{\xi}_m < \delta_m$ where $X = X_m + \epsilon^{(m-2)/2}\gamma_m + \epsilon^{-(m+2)/10}\tilde{\xi}_m$. Here

$$\phi - 1 = \epsilon^{3(m+2)/10} \tilde{\phi}_m(\tilde{\xi}_m) + \cdots, \quad \epsilon \to 0 \tag{4.24}$$

and $\tilde{\phi}_m < 0$ so that $\tilde{\phi}_m$ satisfies the system

$$\tilde{\phi}_m''' + \tilde{\phi}_m^2 = 0; \quad \tilde{\phi}_m = 0, \tilde{\phi}_m'' = (2\beta_m/3)^{1/2} \text{ on } \tilde{\xi}_m = 0, \quad \tilde{\phi}_m = \tilde{\phi}_m'' = 0 \text{ on } \tilde{\xi}_m = \delta_m. \tag{4.25}$$

The conditions at the unknown outer boundary are needed to match with the next outer region, in the same way as those at $X = X_0$ in (4.18). A numerical solution gives

$$\tilde{\phi}_m'(\delta_m) = \beta_{\bar{m}} = 0.387 \left(\frac{2\beta_m}{3}\right)^{2/5}, \quad \delta_m = 3.8 \left(\frac{2\beta_m}{3}\right)^{-1/10}, \tag{4.26}$$

along with $\tilde{\phi}_m'(0) = -1.18(2\beta_m/3)^{2/5}$, which generates a correction to the solution in the outer region. The result (4.26) gives

$$\frac{\partial \phi}{\partial X}(X_{\bar{m}}) = \epsilon^{\bar{m}} \beta_{\bar{m}}, \tag{4.27}$$

where

$$X_{\bar{m}} = X_m + \epsilon^{(m-2)/2}\gamma_m + \epsilon^{-(m+2)/10}\delta_m \tag{4.28}$$

and

$$\bar{m} = \frac{2}{5}(m+2), \tag{4.29}$$

and so is equivalent to (4.20) with m replaced by $\bar{m}$. Thus, the same structure is now repeated with m replaced by $\bar{m}$, implying an infinite sequence of outer/inner regions

with different scalings in ϵ. The main vortex corresponds to $m = 0$ and then successive values implied by the mapping (4.29) are

$$m = \frac{4}{5}, \frac{28}{25}, \frac{156}{125}, \ldots. \tag{4.30}$$

In the limit as the number of regions tends to infinity, the value of m tends to 4/3. At this point the scalings of $\phi - 1$ in (4.21) and (4.24) both become equal to ϵ, the inner and outer scalings in X both become equal to $\epsilon^{-1/3}$ and the right-hand side of (4.14) comes into balance, allowing the solution for $\phi - 1$ to finally approach $-\epsilon$ as $X \to \infty$.

The above structure is consistent with the profile for $\epsilon = 0.05$ obtained numerically in figure 4(b), although the second inner and outer regions have not fully developed at this point. The results for the main vortex ($m = 0$) predict that as $\epsilon \to 0$,

$$\phi_{max} - 1 \sim \epsilon^{-1} \frac{2}{81}(6\beta_0)^{3/2} = 0.160(1 - \phi_\infty)^{-1} \tag{4.31}$$

and this maximum occurs at

$$X - X_0 \sim \epsilon^{-1} \frac{1}{3}(6\beta_0)^{1/2} = 0.621(1 - \phi_\infty)^{-1}. \tag{4.32}$$

The outer boundary of the main vortex is predicted to occur at

$$X - X_0 \sim \epsilon^{-1}(6\beta_0)^{1/2} = 1.86(1 - \phi_\infty)^{-1}. \tag{4.33}$$

The asymptotes (4.31)–(4.33) are shown in figure 5.

The results of this section show that there is a solution in the vertical boundary layer that matches with that in the horizontal boundary layer although both the vertical boundary-layer width and the maximum value of the streamfunction across the layer increase without bound as $\phi_\infty \to 1$, that is as $Z \to Z_0$. From (3.20), (4.4) and (4.8), $\epsilon = 1 - \phi_\infty \sim \Psi_1(Z - Z_0)^2/\Psi_0$ as $Z \to Z_0 \pm$ so that the results (4.31)–(4.33) demonstrate that the vertical boundary layer and vortex width expand, with $X \sim (Z - Z_0)^{-2}$ as $Z \to Z_0 \pm$, and the streamfunction increases in value, with $\phi \sim (Z - Z_0)^{-2}$ as $Z \to Z_0 \pm$, becoming much larger than the streamfunction $\phi \sim 1$ within the horizontal boundary layer. Also, the oscillations of the streamfunction outside the main vortex diminish in amplitude. As Z approaches Z_0, the scale of variation in z becomes comparable with that in x across the main vortex, and the z derivatives can no longer be neglected in comparison with the x derivatives in the vertical boundary-layer equation (4.2). This leads to the main vortex region considered below.

5. Vortex

The scalings implied by the breakdown of the vertical boundary layer as $Z \to Z_0$ lead to a vortex region (region IV in figure 1) in which

$$\psi = R^{11/45}\bar{\phi}(\bar{\xi}, \bar{\zeta}) + \cdots, \quad T = \Theta_0 + R^{-4/45}\bar{\theta}(\bar{\xi}, \bar{\zeta}) + \cdots, \quad R \to \infty, \tag{5.1}$$

where $x = R^{-4/15}\Theta_0^{-1/3}\Psi_0^{1/3}X_0 + R^{-2/9}\bar{\xi}$ and $z = R^{-1/5}Z_0 + R^{-2/9}\bar{\zeta}$ and X_0 and Z_0 are given by (4.19) and (3.19). This region is wider than the vertical boundary layer by a factor of $R^{2/45}$ and shallower by a factor of $R^{-1/45}$, suggesting that extremely large values of R will be needed to resolve this structure in a numerical solution of the full system. Substitution of (5.1) into the governing equations (2.2) and (2.3) shows that $\bar{\theta}$

is a function of $\bar{\phi}$ and that

$$\bar{\nabla}^4\bar{\phi} = \frac{\partial\bar{\theta}}{\partial\bar{\xi}}. \tag{5.2}$$

Matching with the horizontal boundary-layer form for Θ given in (3.20) requires that at large values of $\bar{\xi}$,

$$\bar{\theta} = \bar{\theta}_\infty(\bar{\zeta}) = -\Theta_1\bar{\zeta}^4 \tag{5.3}$$

and inside the vortex where $\bar{\phi} > 0$ it is assumed that $\bar{\theta} = 0$ on the grounds that any constant correction to T of order $R^{-4/45}$ inside the vortex can be subsumed in Θ_0. It is also assumed that no lower positive powers of $\bar{\zeta}$ arise on the right-hand side of (5.3) from possible higher-order contributions in the horizontal boundary layer. It now follows from (5.2) that inside the vortex

$$\int_{\bar{\xi}}^{\infty} \bar{\nabla}^4\bar{\phi}\,\mathrm{d}\bar{\xi} = \bar{\theta}_\infty - \bar{\theta} = -\Theta_1\bar{\zeta}^4. \tag{5.4}$$

Between the vortex and the wall, the inner section of the vertical boundary layer $0 < X < X_0$ must continue unchanged, being generated by the temperature/streamfunction relation for $\phi < 1$, and with $\partial^2\phi/\partial X^2$ zero at $X = X_0$. Matching between the vertical boundary layer and the vortex therefore requires that

$$\bar{\phi} = 0, \quad \frac{\partial\bar{\phi}}{\partial\bar{\xi}} = \bar{\beta}_0 = \beta_0\Psi_0^{2/3}\Theta_0^{1/3} \text{ at } \bar{\xi} = 0, \tag{5.5}$$

where β_0 is given by (4.19). This vertical velocity generates the anticlockwise rotation of the vortex. Finally, it is expected that

$$\bar{\phi} = \frac{\partial\bar{\phi}}{\partial\bar{\xi}} = 0 \text{ at } \bar{\xi} = \bar{s}(\bar{\zeta}), \tag{5.6}$$

where $\bar{s}(\bar{\zeta})$ is the unknown outer boundary of the vortex for $-\infty < \bar{\zeta} < \infty$. From the discussion of the vertical boundary-layer structure as $\epsilon \to 0$ in the previous section, it is expected that the flow in the region $\bar{s} < \bar{\xi} < \infty$ outside the vortex is extremely complex and it is not attempted to analyse that here.

The vortex problem (5.4)–(5.6) can be simplified by scaling out the constants $\bar{\beta}_0$ and Θ_1 using the transformations

$$(\bar{\xi}, \bar{\zeta}) = \bar{\beta}_0^{1/6}\Theta_1^{-1/6}(\xi, \zeta), \quad \bar{\phi}(\bar{\xi}, \bar{\zeta}) = \bar{\beta}_0^{7/6}\Theta_1^{-1/6}\Phi(\xi, \zeta), \quad \bar{s}(\bar{\zeta}) = \bar{\beta}_0^{1/6}\Theta_1^{-1/6}s(\zeta). \tag{5.7}$$

This gives the system

$$\frac{\partial^3\Phi}{\partial\xi^3} + 2\frac{\partial^3\Phi}{\partial\xi\,\partial\zeta^2} - \int_{\xi}^{s(\zeta)} \frac{\partial^4\Phi}{\partial\zeta^4}\mathrm{d}\xi = \zeta^4, \tag{5.8}$$

$$\Phi = 0, \frac{\partial\Phi}{\partial\xi} = 1 \text{ at } \xi = 0, \tag{5.9}$$

$$\Phi = 0, \frac{\partial\Phi}{\partial\xi} = 0 \text{ at } \xi = s(\zeta). \tag{5.10}$$

This is a nonlinear problem for Φ and s and a complete solution would require a numerical approach. This is not attempted here, but progress can be made analytically by using an approximation based on a power-series expansion in ξ. From (5.9), the streamfunction can be expressed in the form

$$\Phi = \xi + a(\zeta)\xi^2 + b(\zeta)\xi^3 + \cdots \tag{5.11}$$

and substitution in (5.8) gives at leading order

$$6b - \frac{1}{3}a''''s^3 - \frac{1}{4}b''''s^4 = \zeta^4. \tag{5.12}$$

The outer conditions (5.10) give

$$a = -2s^{-1}, \quad b = s^{-2}, \tag{5.13}$$

and then (5.12) can be written in the form

$$v'''' = 6(\zeta^4 - 6v^2)v^3 + (9v''^2 + 12v'v''')v^{-1}, \tag{5.14}$$

where $v = s^{-1}$. Matching with the vertical boundary layer requires that

$$v \sim \zeta^2/\sqrt{6} \text{ as } \zeta \to \pm\infty. \tag{5.15}$$

Exponentially small terms in the asymptotic form (5.15) have the form $\mu\zeta^3 e^{-\omega\zeta^3}\cos(\omega\zeta^3 + \Omega)$ as $\zeta \to \infty$, where $\omega = 2^{-1/4}/3$ and μ and Ω are arbitrary constants. Correct choice of μ and Ω leads to an even solution for v consistent with symmetry conditions $v' = v''' = 0$ at $\zeta = 0$.

A numerical solution of (5.14) and (5.15) was obtained using a fourth-order Runge–Kutta scheme. The solution was computed outwards from the conditions $v = \bar{A}$, $v' = 0$, $v'' = \bar{B}$, $v''' = 0$ at $\zeta = 0$ and the values of $\bar{A}$ and $\bar{B}$ found by Newton iteration based on satisfaction of the boundary conditions $v'' = 2/\sqrt{6}$, $v''' = 0$ at $\zeta = \zeta_\infty$. In order to achieve convergence, it was necessary to start the scheme with a low value of $\zeta_\infty (= 1/2)$ and initial values $\bar{A} = 6^{-1/6}$, $\bar{B} = 2/\sqrt{6}$ were used corresponding to an approximate solution $v = 6^{-1/6} + \zeta^2/\sqrt{6}$ based on a small ζ expansion. Convergence was achieved, $\bar{A}$ and $\bar{B}$ were updated, and then ζ_∞ was increased in steps of 0.1 to obtain an accurate solution for v, which is shown in figure 6(a) and corresponds to $\bar{A} = v(0) = 0.559$, $\bar{B} = v''(0) = 0.378$. From (5.11) and (5.13), $\Phi = \xi(1 - s^{-1}\xi)^2$ and the streamfunction attains its maximum value at the centre of the vortex where $\zeta = 0$,

$$\Phi = \Phi_0 = \frac{4}{27}s(0) = \frac{4}{27}v(0)^{-1} = 0.265 \tag{5.16}$$

and

$$\xi = \xi_0 = \frac{1}{3}s(0) = \frac{1}{3}v(0)^{-1} = 0.596. \tag{5.17}$$

Figure 6(b) shows the streamlines of the vortex in the ξ, ζ plane. As $\zeta \to \pm\infty$, the vortex boundary has the behaviour $\xi = s(\zeta) \sim \sqrt{6}\zeta^{-2}$. The small ξ expansion (5.11) is then formally correct to leading order and matches with the vertical boundary-layer form (4.33) as $Z \to Z_0\pm$ which, in turn, is consistent with the solution in the horizontal boundary layer surrounding the vortex.

6. Inner vertical layer

Thermal conduction is too small to influence the leading-order solution in the main vertical layer and vortex, but becomes significant in an inner vertical layer adjacent to the cold sidewall (region V in figure 1). In this region the flow field is that supplied by the main vertical boundary-layer solution as $\bar{X} \to 0$ and to a first approximation buoyancy can be neglected in the vorticity equation. Matching with the main vertical boundary layer and balancing conduction with convection then requires

$$\psi = R^{1/9}\hat{\Psi}(\hat{X}, Z) + \cdots, \quad T = R^{-4/45}\hat{\Theta}(\hat{X}, Z) + \cdots, \quad R \to \infty, \tag{6.1}$$

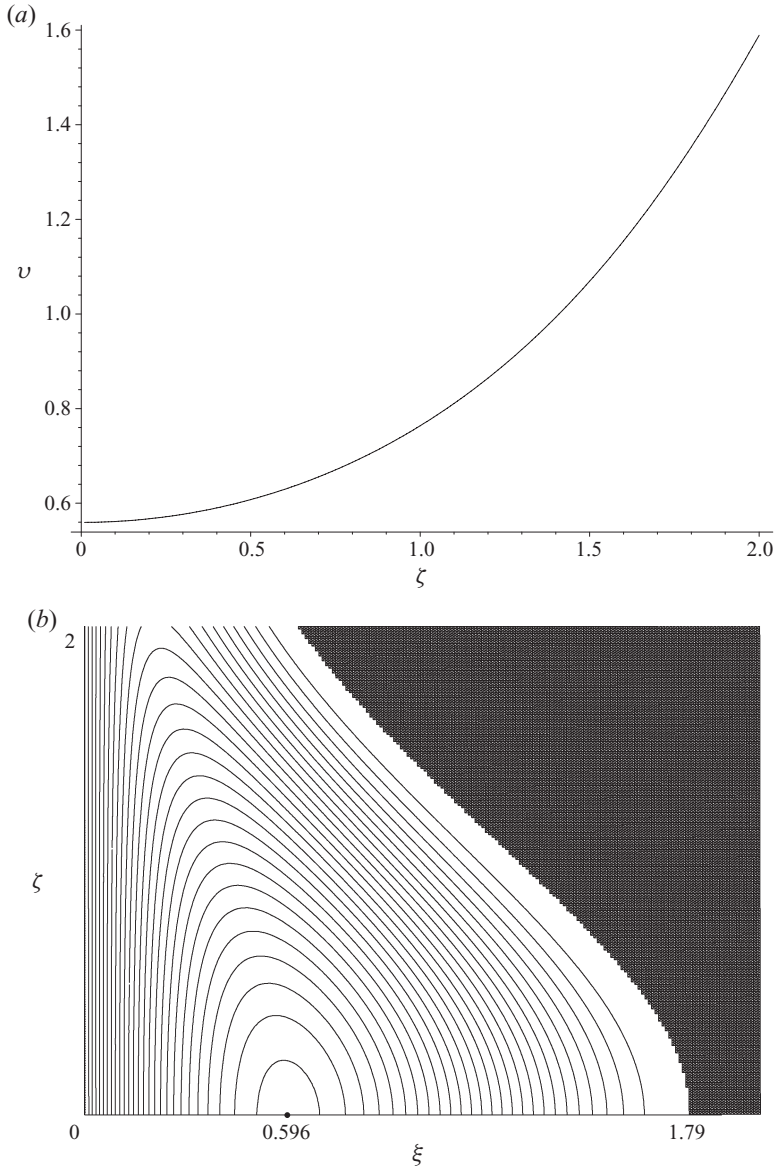

FIGURE 6. Solution in the vortex region showing (a) the vortex function $v(\zeta)$ obtained from the solution of (5.14) and (5.15) and (b) streamlines of the vortex in the ξ, ζ plane, shown at intervals in Φ of 0.01. The solution is symmetric about $\zeta = 0$, with downward flow at the wall.

where $x = R^{-14/45}\hat{X}$. Substitution in (2.2) gives $\partial^4\hat{\Psi}/\partial\hat{X}^4 = 0$ and the required solution that satisfies the wall conditions $\hat{\Psi} = \partial\hat{\Psi}/\partial\hat{X} = 0$ at $\hat{X} = 0$ and matches with the main vertical layer solution is

$$\hat{\Psi} = \hat{a}(Z)\hat{X}^2, \tag{6.2}$$

where $2\hat{a}(Z) = \partial^2\bar{\Psi}/\partial\bar{X}^2(\bar{X}=0) = \Psi_0^{1/3}\Theta_0^{2/3}\partial^2\phi/\partial X^2(X=0) = \Psi_0^{1/3}\Theta_0^{2/3}\alpha$ and α is given as a function of ϕ_∞ in figure 5(a). From (2.3) and (6.2), $\hat{\Theta}$ satisfies the

equation

$$\frac{\partial^2\hat{\Theta}}{\partial\hat{X}^2} = 2\hat{a}\hat{X}\frac{\partial\hat{\Theta}}{\partial Z} - \hat{a}'\hat{X}^2\frac{\partial\hat{\Theta}}{\partial\hat{X}}. \tag{6.3}$$

The wall condition (2.6) requires that

$$\frac{\partial\hat{\Theta}}{\partial\hat{X}} = 0 \text{ at } \hat{X} = 0 \tag{6.4}$$

and matching with the main vertical layer requires that

$$\hat{\Theta} \sim K\hat{a}\hat{X}^2 \text{ as } \hat{X} \to \infty. \tag{6.5}$$

The temperature in this wall layer is larger as $R \to \infty$ than that given by the surface profile (3.17) and so

$$\hat{\Theta} = 0 \text{ at } Z = 0. \tag{6.6}$$

The solution of (6.3)–(6.6) can be found by transforming the independent variables from $(\hat{X}, Z)$ to $(\hat{\Psi}, \hat{Z})$, where $\hat{Z}$ is defined by

$$\hat{Z} = \int_0^Z \{\hat{a}(Z)\}^{1/2}\mathrm{d}Z. \tag{6.7}$$

This gives the system

$$2\hat{\Psi}\frac{\partial^2\hat{\Theta}}{\partial\hat{\Psi}^2} + \frac{\partial\hat{\Theta}}{\partial\hat{\Psi}} = \hat{\Psi}^{1/2}\frac{\partial\hat{\Theta}}{\partial\hat{Z}}, \tag{6.8}$$

$$\frac{\partial\hat{\Theta}}{\partial(\hat{\Psi}^{1/2})} = 0 \text{ at } \hat{\Psi} = 0, \qquad \hat{\Theta} \sim K\hat{\Psi} \text{ as } \hat{\Psi} \to \infty, \tag{6.9}$$

$$\hat{\Theta} = 0 \text{ at } \hat{Z} = 0. \tag{6.10}$$

This is solved by the similarity form

$$\hat{\Theta} = K\hat{Z}^{2/3}H(\hat{\eta}), \quad \hat{\eta} = \hat{\Psi}^{1/2}/\hat{Z}^{1/3}, \tag{6.11}$$

where

$$H'' + \frac{2}{3}\hat{\eta}^2H' - \frac{4}{3}\hat{\eta}H = 0; \quad H'(0) = 0, \quad H \sim \hat{\eta}^2, \quad \hat{\eta} \to \infty. \tag{6.12}$$

A numerical solution was obtained by computing outwards from a finite value of H at $\hat{\eta} = 0$ and is shown in figure 7. It has the property that $H(0) = H_0 = 1.797$ so that the scaled wall temperature is determined as $\hat{\Theta} = K\hat{Z}^{2/3}H_0$.

It is known from the main vertical layer solution (4.5) that $\hat{a}(Z)$ has the form

$$\hat{a} \sim \frac{1}{2}K^{2/3}a_1Z, \qquad Z \to 0; \quad \hat{a} \sim K^{2/3}Z^{-1}, \qquad Z \to \infty. \tag{6.13}$$

Thus, the width of the inner vertical layer remains finite as $Z \to 0$. In fact, although modifications to this inner vertical layer solution might be expected within a corner region where the full heat equation (2.3) comes into play, the second-order z derivative in the Laplacian of the temperature field does not affect the leading-order contribution to (6.11) as $Z \to 0$ which therefore remains a uniformly valid first approximation to the solution at depths of order $R^{-14/45}$ from the upper surface.

As $Z \to \infty$, the temperature in the inner vertical layer rises ($\hat{\Theta} \sim Z^{1/3}$) and the layer spreads, with $\hat{X} \sim Z^{2/3}$. From (4.5) the outer vertical layer thickness remains finite as $Z \to \infty$, and it follows that the two vertical layers merge at a depth z of order

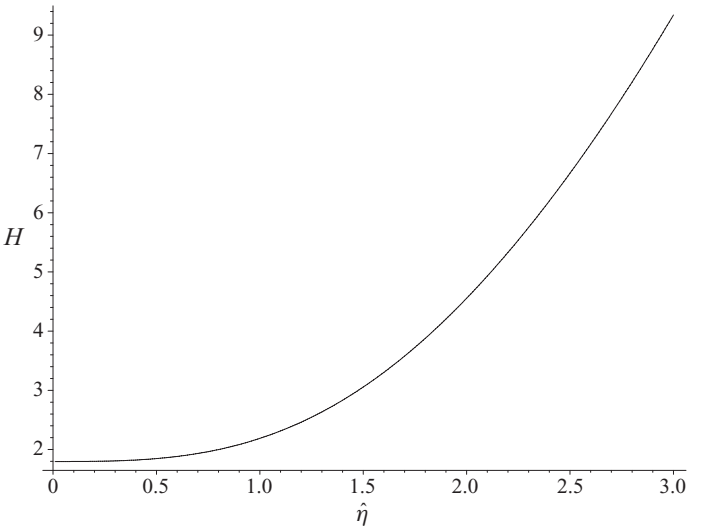

FIGURE 7. The inner vertical layer function $H(\hat{\eta})$ for a shear-free upper surface, given by the solution of (6.12).

$R^{-2/15}$. This leads to a new horizontal structure across the cavity which is considered in the next section.

7. Plume and outer horizontal layer

The two vertical layers merge in the plume (region VI in figure 1) where

$$\psi = R^{2/15}K^{1/6}\tilde{\psi}(\tilde{X},\tilde{Z}) + \cdots, \quad T = R^{-1/15}K^{7/6}\tilde{T}(\tilde{X},\tilde{Z}) + \cdots, \quad R \to \infty \tag{7.1}$$

and

$$x = R^{-4/15}K^{-1/3}\tilde{X}, \quad z = R^{-2/15}K^{-1/6}\tilde{Z}. \tag{7.2}$$

Substitution in (2.2) and (2.3) shows that the flow is governed by the full vertical boundary-layer equations

$$\frac{\partial^3\tilde{\psi}}{\partial\tilde{X}^3} = \tilde{T} - \tilde{T}_\infty, \tag{7.3}$$

$$\frac{\partial^2\tilde{T}}{\partial\tilde{X}^2} = \frac{\partial\tilde{\psi}}{\partial\tilde{X}}\frac{\partial\tilde{T}}{\partial\tilde{Z}} - \frac{\partial\tilde{\psi}}{\partial\tilde{Z}}\frac{\partial\tilde{T}}{\partial\tilde{X}}, \tag{7.4}$$

so that friction, buoyancy, conduction and convection are all significant. The boundary conditions are

$$\tilde{\psi} = \frac{\partial\tilde{\psi}}{\partial\tilde{X}} = \frac{\partial\tilde{T}}{\partial\tilde{X}} = 0 \text{ at } \tilde{X} = 0, \tag{7.5}$$

$$\tilde{\psi} \to \tilde{\psi}_\infty(\tilde{Z}), \quad \tilde{T} \to \tilde{T}_\infty(\tilde{Z}) \text{ as } \tilde{X} \to \infty \tag{7.6}$$

and, from matching with the outer and inner vertical layers, respectively,

$$\tilde{\psi} \sim 2\tilde{Z}^{-1}f(\tilde{X}), \quad \tilde{T} \sim 2\tilde{Z}^{-1}f(\tilde{X}), \quad \tilde{X} \sim 1, \tag{7.7}$$

and

$$\tilde{\psi} \sim \tilde{Z}^{1/3}\eta^2, \quad \tilde{T} \sim 2^{2/3}\tilde{Z}^{1/3}H(\eta/2^{1/3}), \quad \eta = \tilde{X}/\tilde{Z}^{2/3} \sim 1, \tag{7.8}$$

as $\tilde{Z} \to 0$, where f is given by (4.5). The final requirement comes from matching with a stratified flow in the outer horizontal layer (region VII in figure 1) where

$$\psi = R^{2/15}K^{1/6}(1-x)\tilde{\psi}_\infty(\tilde{Z}) + \cdots, \quad T = R^{-1/15}K^{7/6}\tilde{T}_\infty(\tilde{Z}) + \cdots, \quad R \to \infty \tag{7.9}$$

and

$$\tilde{\psi}_\infty = -\frac{\tilde{T}''_\infty}{\tilde{T}'_\infty}. \tag{7.10}$$

Here vertical conduction and convection are in balance, buoyancy dominates in the vorticity equation and detrainment from the plume generates motion up and across the cavity into the main horizontal boundary layer. Note that the inner form of $\tilde{T}$ in (7.8) precludes the possibility of a non-zero constant contribution to $\tilde{T}$ across the layer as $\tilde{Z} \to 0$. Note also that inclusion of K in the scalings (7.1) and (7.2) allows it to be removed from the plume problem (7.3)–(7.8) and (7.10), which must be solved to determine the vertical flow and temperature fields $\tilde{\psi}_\infty(\tilde{Z})$ and $\tilde{T}_\infty(\tilde{Z})$ in the outer horizontal layer. A full solution would require a numerical approach and, given the singular form (7.7) and (7.8) as $\tilde{Z} \to 0$ and the existence of flow reversals in the velocity profile, is a non-trivial problem. It is known from matching with the main horizontal layer that

$$\tilde{\psi}_\infty \sim 2\tilde{Z}^{-1}, \quad \tilde{T}_\infty \sim 2\tilde{Z}^{-1} \text{ as } \tilde{Z} \to 0 \tag{7.11}$$

and, as $\tilde{Z} \to \infty$, the asymptotic solution described by Chiu-Webster *et al.* (2008) should emerge, with

$$\tilde{\psi}_\infty \sim \frac{8}{\tilde{Z}+\tilde{Z}_c}, \quad \tilde{T}_\infty \sim \tilde{T}_c + \frac{c}{(\tilde{Z}+\tilde{Z}_c)^7}, \quad \tilde{Z} \to \infty, \tag{7.12}$$

where $c = 6610$. The plume also contains variations in $\tilde{\psi}$ and $\tilde{T}$ of order $(\tilde{Z}+\tilde{Z}_c)^{-1}$ and $(\tilde{Z}+\tilde{Z}_c)^{-7}$, respectively, and expands such that $\tilde{X} \sim (\tilde{Z}+\tilde{Z}_c)^2$ as $\tilde{Z} \to \infty$.

The vertical displacement $\tilde{Z}_c$ and the core temperature coefficient $\tilde{T}_c$ are not determined by the asymptotic analysis for large $\tilde{Z}$ and instead must be determined from the overall solution of the plume problem. An estimate of their values can be obtained by patching the two asymptotic forms (7.11) and (7.12) at an intermediate value of $\tilde{Z}$. Taking this to be $\tilde{Z}_0$ and requiring continuity of $\tilde{\psi}_\infty$, $\tilde{T}_\infty$ and $\tilde{T}'_\infty$ gives

$$\frac{2}{\tilde{Z}_0} = \frac{8}{\tilde{Z}_0+\tilde{Z}_c}, \quad \frac{2}{\tilde{Z}_0} = \tilde{T}_c + \frac{c}{(\tilde{Z}_0+\tilde{Z}_c)^7}, \quad \frac{2}{\tilde{Z}_0^2} = \frac{7c}{(\tilde{Z}_0+\tilde{Z}_c)^8}. \tag{7.13}$$

It follows that $\tilde{Z}_0 = \tilde{Z}_c/3, \tilde{Z}_c = 3(14c)^{1/6}/8 = 2.522$ and the core temperature coefficient is determined as $\tilde{T}_c = 48(14c)^{-1/6}/7 = 1.020$. Thus, it is predicted that the temperature in the core region is

$$T \sim 1.020K^{7/6}R^{-1/15} \text{ as } R \to \infty. \tag{7.14}$$

A local adjustment of the outer horizontal layer solution (7.9) also occurs near the hot sidewall (region VIII in figure 1) to adjust the vertical velocity to zero. This is similar in form to the corresponding end region for the main horizontal layer (region II) and the local solution is given by

$$\psi = R^{-2/15}\tilde{\Phi}(\tilde{x}, \tilde{Z}) + \cdots, \quad T = R^{-1/15}K^{7/6}\tilde{T}_\infty(\tilde{Z}) + \cdots, \quad R \to \infty, \tag{7.15}$$

where $x = 1 - R^{-4/15}\tilde{x}$ and

$$\tilde{\Phi} = K^{1/6}\tilde{\lambda}^{-1}\frac{\mathrm{d}\tilde{\lambda}}{\mathrm{d}\tilde{Z}}\left\{-\tilde{x} + \sqrt{2}K^{-1/3}\tilde{\lambda}^{-1/4}\mathrm{e}^{-\tilde{\lambda}^{1/4}K^{1/3}\tilde{x}/\sqrt{2}}\sin(\tilde{\lambda}^{1/4}K^{1/3}\tilde{x}/\sqrt{2})\right\}, \tag{7.16}$$

where $\tilde{\lambda} = -\tilde{T}'_\infty(\tilde{Z}) > 0$. Since $\tilde{T}'_\infty$ is of order $(\tilde{Z}+\tilde{Z}_c)^{-8}$ as $\tilde{Z} \to \infty$ this hot wall layer expands such that $\tilde{x} \sim (\tilde{Z}+\tilde{Z}_c)^2$, the same order of magnitude as the expansion of the plume on the other side of the cavity. For both layers the overall scale in x is of order $R^{-4/15}\tilde{Z}^2$ so that when $\tilde{Z} \sim R^{2/15}$, equivalent to $z \sim 1$, the boundary-layer widths are comparable with the cavity width $x \sim 1$. Thus, the boundary layers and the stratified interior merge within the main core region of the cavity (region IX in figure 1), where

$$\psi = \psi_c(x,z)+\cdots, \quad T = \{R^{-1/15}K^{7/6}\tilde{T}_c+\cdots\}+R^{-1}T_c(x,z)+\cdots, \quad R \to \infty \tag{7.17}$$

and ψ_c and T_c satisfy the full equations (2.2) and (2.3) with R scaled out. Thus, the core region contains a weakly recirculating flow, with temperature variations limited to order R^{-1}. The terms in the parentheses in (7.17) indicate constant contributions to the temperature field, the leading contribution being that determined in (7.14).

8. Rigid upper surface

If the shear-free upper surface is replaced by a rigid upper surface, a similar asymptotic structure occurs but the length scales in the Rayleigh number associated with the outer horizontal structure are slightly different, as shown in figure 8. This leads to a core temperature of order $R^{-2/65}$ rather than $R^{-1/15}$. In this section, the main features of the structure for the rigid case are described.

The main horizontal layer is governed by (3.1)–(3.6) except that (3.3) is replaced by

$$\Psi = \frac{\partial \Psi}{\partial Z} = 0, \quad \Theta = S(x) \text{ on } Z = 0. \tag{8.1}$$

This has the consequence that the small-Z expansions of Ψ and Θ at $x = 0$ in (3.12) are replaced by

$$\Psi = a_2 Z^2 + a_3 Z^3 + a_4 Z^4 + \cdots, \quad \Theta = b_1 Z + b_3 Z^3 + \cdots \tag{8.2}$$

and so (3.13) is replaced by

$$F(\Psi) = K\Psi^{1/2} + L\Psi + M\Psi^{3/2} + \cdots \text{ as } \Psi \to 0, \tag{8.3}$$

where $K = b_1/a_2^{1/2} > 0$, $L = -b_1 a_3/2a_2^2$, and so on. It follows that as $Z \to \infty$,

$$\Psi = \frac{3(1-x)}{2Z} + \frac{3\sqrt{3}LK^{-1}(1-x)}{2\sqrt{2}Z^{3/2}} + \frac{27(MK^{-1}-(5/8)L^2K^{-2})(1-x)\ln Z}{10Z^2} + O(Z^{-2}), \tag{8.4}$$

$$\Theta = \frac{\sqrt{3}K}{(2Z)^{1/2}} + \frac{9L}{4Z} + \frac{9\sqrt{3}(M-(5/8)L^2K^{-1})\ln Z}{10\sqrt{2}Z^{3/2}} + O(Z^{-3/2}) \tag{8.5}$$

for $0 \leqslant x \leqslant 1$ in place of (3.14). The horizontal boundary-layer problem was solved numerically using the form of Ψ in (8.4) as an outer boundary condition but with Z replaced by $Z + D$ to include the possibility of an origin shift, and the values of K, L and M obtained by fitting (8.3) at the grid points $Z = \Delta Z, 2\Delta Z, 3\Delta Z$ on $x = 0$. An initial state

$$\Psi = \frac{3Z^2(1-x)}{2(1+Z^3)}, \quad \Theta = S(x)\mathrm{e}^{-Z} + \frac{\sqrt{3}KZ}{\sqrt{2}(1+Z^3)^{1/2}} \tag{8.6}$$

was used at $t = 0$, with K in the range 0.2 to 0.5. In other respects, the calculations were similar to those for the shear-free case and the most accurate results with

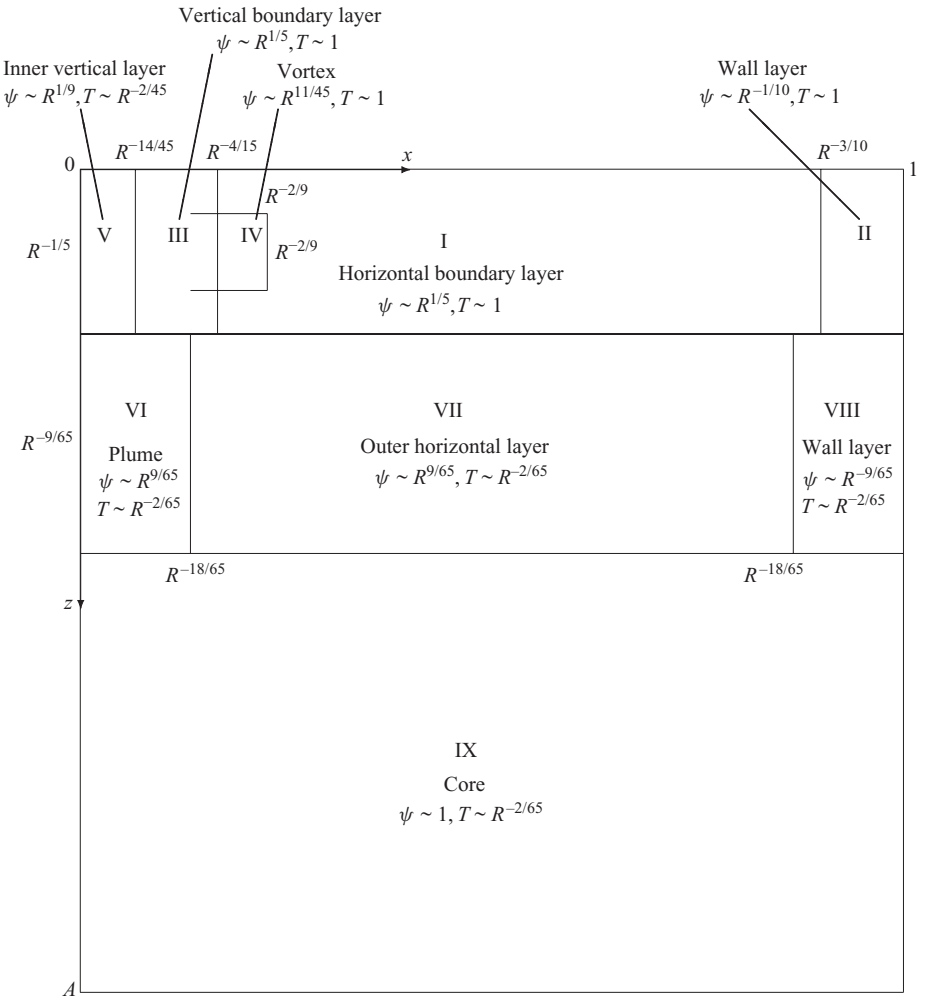

FIGURE 8. Schematic diagram of the main regions of the asymptotic structure of the solution for a rigid upper surface in the limit $R \to \infty$. The leading-order scalings of ψ and T in each region are shown.

$\Delta X = 0.05$, $\Delta Z = 0.2$, $Z_\infty = 30$, $\Delta t = 0.0001$ and $t_\infty = 1000$ for the linear profile $S(x) = x$ gave a steady-state solution with

$$K = 0.434, \quad L = 0.425, \quad M = -0.742, \tag{8.7}$$

maximum values of Θ and Ψ on $x = 0$ given by

$$\Psi = \Psi_0 = 0.560, \quad \Theta = \Theta_0 = 0.288 \text{ at } Z = Z_0 = 2.82 \tag{8.8}$$

and $Nu_0 = 0.17$. The streamlines and isotherms are shown in figure 9 and the profiles of Ψ and Θ at $x = 0$ in figure 10 along with the function $F(\Psi)$. The forms (3.20) remain valid near $Z = Z_0$ but with

$$\Psi_1 = 0.090, \quad \Theta_1 = 0.0037 \tag{8.9}$$

and the vortex structure near Z_0 is expected to be similar to that for the shear-free problem. The approximation (4.6) to F is no longer appropriate near $\bar{\Psi} = 0$ and can

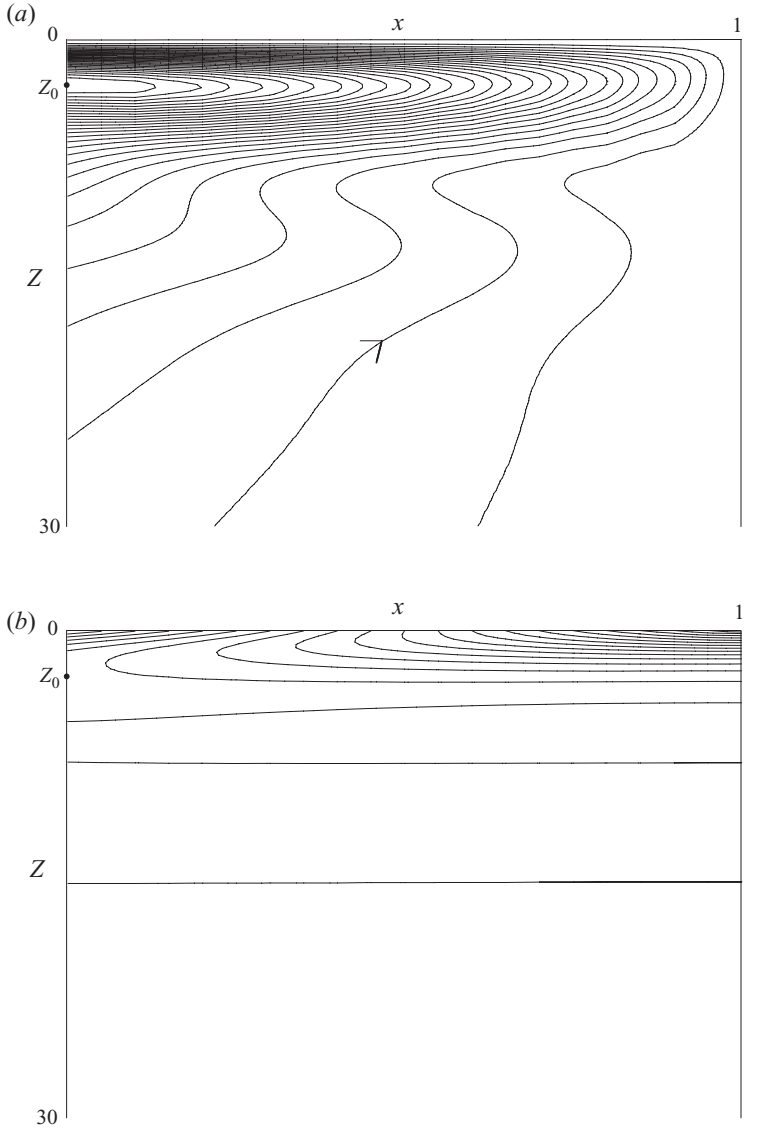

FIGURE 9. Streamlines (*a*) and isotherms (*b*) of the horizontal boundary-layer solution for a rigid upper surface with a linear temperature profile. Intervals in Ψ and Θ are 0.02 and 0.05, respectively. The point $Z_0 = 2.82$ is shown.

be replaced by

$$F(\bar{\Psi}) = \frac{\Theta_0 \bar{\Psi}^{1/2}\left(4\Psi_0^{3/2} - \bar{\Psi}^{3/2}\right)}{3\Psi_0^2}, \quad 0 \leqslant \bar{\Psi} \leqslant \Psi_0, \tag{8.10}$$

to good effect (see figure 10). This leads to new values of β_0 and X_0 in (4.19) given by

$$X_0 = 2.56, \quad \beta_0 = \tilde{\phi}'(X_0) = 0.545. \tag{8.11}$$

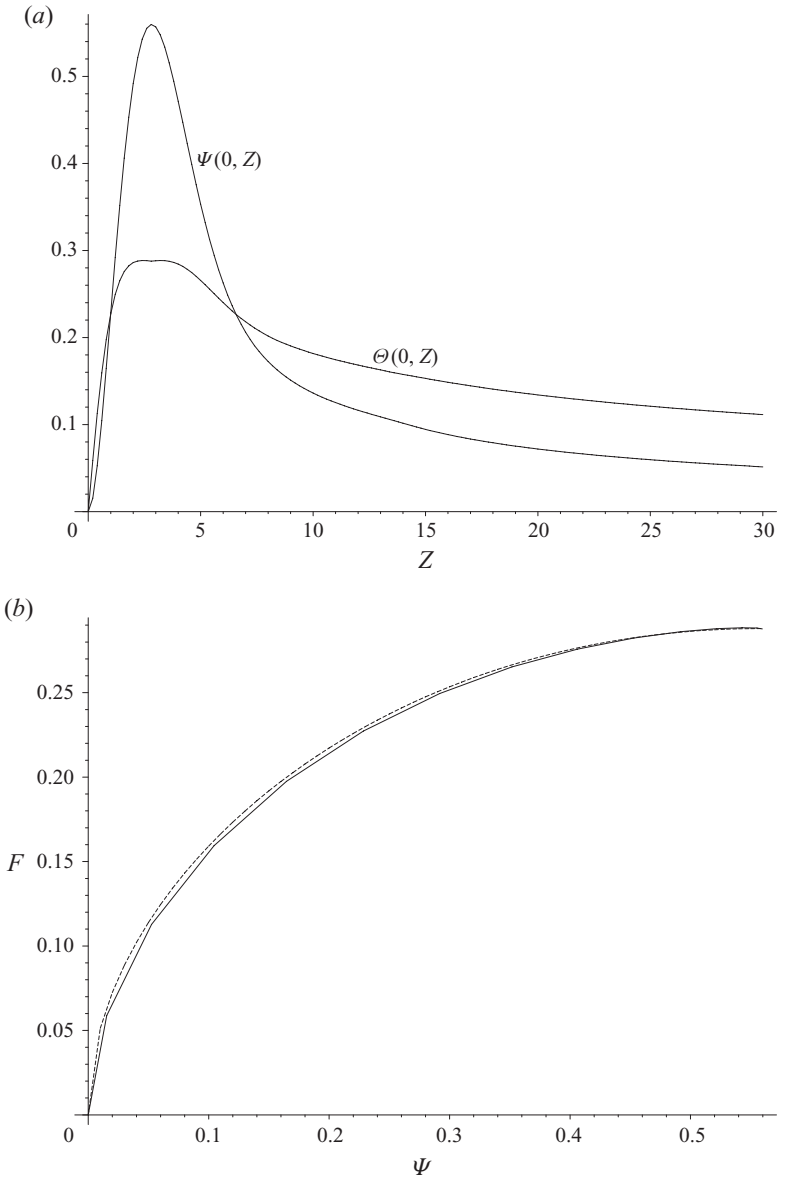

FIGURE 10. Horizontal boundary-layer solution for a rigid upper surface with a linear temperature profile showing (*a*) the profiles $\Psi(0, Z)$ and $\Theta(0, Z)$ and (*b*) the function $F(\Psi)$ along with the analytical approximation (8.10) (- - -).

Since now $\bar{\Theta} = F(\bar{\Psi}) \sim K\bar{\Psi}^{1/2}$ as $\bar{\Psi} \to 0$ the temperature in the inner vertical layer (region V in figure 8) is larger than that in the shear-free case, with

$$\psi = R^{1/9}\hat{\Psi}(\hat{X}, Z) + \cdots, \quad T = R^{-2/45}\hat{\Theta}(\hat{X}, Z) + \cdots, \quad R \to \infty, \tag{8.12}$$

in place of (6.1). With $\hat{\Psi} = \hat{a}\hat{X}^2$, the problem for $\hat{\Theta}$ is again defined by (6.3)–(6.6) except that (6.5) is replaced by

$$\hat{\Theta} \sim K\hat{a}^{1/2}\hat{X}, \quad \hat{X} \to \infty \tag{8.13}$$

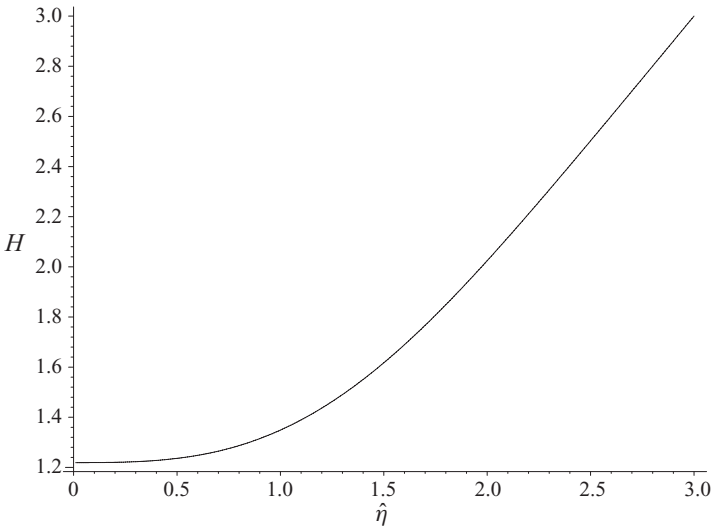

FIGURE 11. The inner vertical layer function $H(\hat{\eta})$ for a rigid upper surface given by (8.15).

and the relevant similarity solution is now

$$\hat{\Theta} = K\hat{Z}^{1/3}H(\hat{\eta}), \quad \hat{\eta} = \hat{\Psi}^{1/2}/\hat{Z}^{1/3}, \tag{8.14}$$

where $\hat{Z}$ is given by (6.7),

$$H(\hat{\eta}) = \hat{\eta}\left\{1 + \frac{1}{3\Gamma(2/3)}\int_{2\hat{\eta}^3/9}^{\infty} v^{-4/3}\mathrm{e}^{-v}\mathrm{d}v\right\} \tag{8.15}$$

and Γ is the gamma function (Abramowitz & Stegun 1965, p. 253). This determines the scaled wall temperature as $\hat{\Theta} = K\hat{Z}^{1/3}H_0$ where $H_0 = H(0) = (9/2)^{1/3}/\Gamma(2/3) = 1.219$. The function H is shown in figure 11.

From the behaviour of the solution in the outer vertical layer as $\bar{\Psi} \to 0$, it follows that

$$\hat{a} \sim K^{2/3}c_0 a_2^{2/3}Z^{4/3}, \quad Z \to 0; \quad \hat{a} \sim K^{2/3}c_\infty Z^{-2/3}, \quad Z \to \infty. \tag{8.16}$$

Here $c_\infty = (3/2)^{2/3}c_0$ can be found from a solution of the outer problem for small $\bar{\Psi}$, which has the form

$$\bar{\Psi} \sim \bar{\Psi}_\infty f(K^{1/3}\bar{\Psi}_\infty^{-1/6}\bar{X}), \qquad \bar{\Psi}_\infty \to 0, \tag{8.17}$$

where f is a function that can be determined numerically and gives $2c_0 = f''(0) = 0.849$. The inner vertical layer expands as $Z \to 0$ (with $\hat{X} \sim Z^{-1/9}$) and as $Z \to \infty$ the temperature rises ($\hat{\Theta} \sim Z^{2/9}$) and the layer again expands ($\hat{X} \sim Z^{5/9}$). In contrast, it follows from (8.17) that the outer vertical layer contracts as $Z \to \infty$, with $\bar{X} \sim Z^{-1/6}$.

The two vertical layers merge in the plume (region VI in figure 8), where (7.1) and (7.2) are replaced by

$$\psi = R^{9/65}K^{2/13}\tilde{\psi}(\tilde{X}, \tilde{Z}) + \cdots, \quad T = R^{-2/65}K^{14/13}\tilde{T}(\tilde{X}, \tilde{Z}) + \cdots, \quad R \to \infty, \tag{8.18}$$

where

$$x = R^{-18/65}K^{-4/13}\tilde{X}, \quad z = R^{-9/65}K^{-2/13}\tilde{Z}. \tag{8.19}$$

The plume equations and boundary conditions are again given by (7.3)–(7.8) and (7.10) except that (7.7) and (7.8) are replaced by

$$\tilde{\psi} \sim \frac{3}{2}\tilde{Z}^{-1} f((2/3)^{1/6}\tilde{\eta}), \quad \tilde{T} \sim \sqrt{3}(2\tilde{Z})^{-1/2}(f((2/3)^{1/6}\tilde{\eta}))^{1/2}, \quad \tilde{\eta} = \tilde{X}\tilde{Z}^{1/6} \sim 1 \tag{8.20}$$

and

$$\tilde{\psi} \sim c_\infty \tilde{Z}^{4/9}\eta^2, \quad \tilde{T} \sim (9c_\infty/4)^{1/6}\tilde{Z}^{2/9} H((2c_\infty/3)^{1/3}\eta), \quad \eta = \tilde{X}/\tilde{Z}^{5/9} \sim 1, \tag{8.21}$$

where H is given by (8.15).

The outer horizontal layer solution (7.9) is now given by

$$\psi = R^{9/65}K^{2/13}\tilde{\psi}_\infty(\tilde{Z})(1-x) + \cdots, \quad T = R^{-2/65}K^{14/13}\tilde{T}_\infty(\tilde{Z}), \quad R \to \infty, \tag{8.22}$$

with

$$\tilde{\psi}_\infty \sim \frac{3}{2\tilde{Z}}, \quad \tilde{T}_\infty \sim \frac{\sqrt{3}}{(2\tilde{Z})^{1/2}}, \quad \tilde{Z} \to 0 \tag{8.23}$$

and the asymptotic solution (7.12) is again expected to emerge as $\tilde{Z} \to \infty$. The approximate method of finding the vertical displacement $\tilde{Z}_c$ and the core temperature coefficient $\tilde{T}_c$ now requires

$$\frac{3}{2\tilde{Z}_0} = \frac{8}{\tilde{Z}_0 + \tilde{Z}_c}, \quad \frac{\sqrt{3}}{(2\tilde{Z}_0)^{1/2}} = \tilde{T}_c + \frac{c}{(\tilde{Z}_0 + \tilde{Z}_c)^7}, \quad \frac{\sqrt{3}}{(2\tilde{Z}_0)^{3/2}} = \frac{7c}{(\tilde{Z}_0 + \tilde{Z}_c)^8}, \tag{8.24}$$

giving $\tilde{Z}_0 = 3\tilde{Z}_c/13$, $\tilde{Z}_c = 13(84c)^{2/13}/32 = 3.109$ and $\tilde{T}_c = 52(84c)^{-1/13}/21 = 0.895$. Thus, the core temperature for a rigid upper surface is predicted to be

$$T \sim 0.895K^{14/13}R^{-2/65} \text{ as } R \to \infty. \tag{8.25}$$

9. Discussion

An asymptotic structure in the limit of large Rayleigh number has been found for the thermally driven flow generated by a monotonic temperature differential along the upper surface of a rectangular cavity containing an infinite Prandtl number fluid. The structure is expected to have the same form for any temperature profile provided the profile is monotonic, so that the descending motion and vortex centre occur near the cold sidewall. Detailed calculations of the main horizontal boundary-layer solution, at depths of order $R^{-1/5}$, are described for a linear temperature profile and for both shear-free and rigid upper surfaces. The main circulation, of order $R^{1/5}$ in the streamfunction, is completed near the cold sidewall within the vertical boundary-layer width of order $R^{-4/15}$, although this drives a vortex in which locally the streamfunction rises to higher values, of order $R^{11/45}$ and within which the temperature is uniform. The main properties of the vertical boundary layer are identified and an approximate solution for the vortex is found. An inner vertical boundary layer of width order $R^{-14/45}$ contains a further adjustment of the temperature field which is determined analytically. Here the temperature increases with depth at the wall, whereas farther out it decreases with depth below a line extending through the vertices of the isotherms in the horizontal boundary layer (see figures 2 and 9).

The inner and outer vertical layers merge at a depth of order $R^{-2/15}$ in the shear-free case, and $R^{-9/65}$ in the rigid case, forming a plume in which the temperature saturates at its core value. On this scale the interior flow is vertically stratified, with the vertical velocity and temperature gradients determined by solving the full vertical

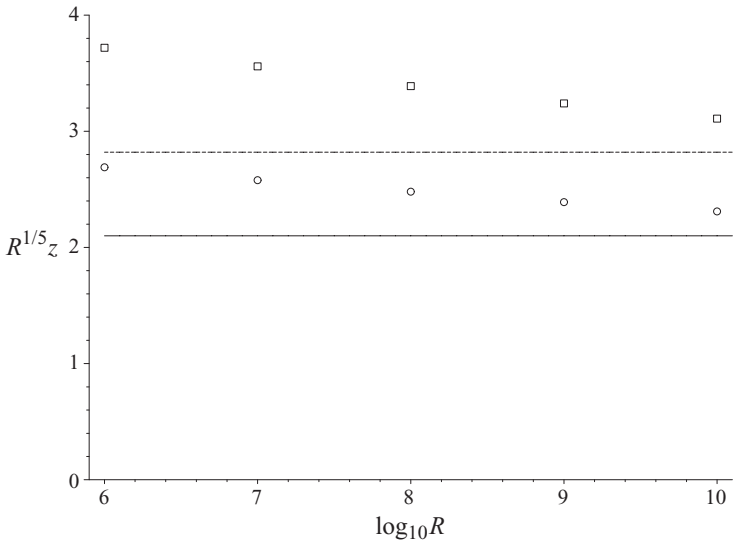

FIGURE 12. The scaled depth of the vortex centre $R^{1/5}z$ given by the computations of Chiu-Webster *et al.* (2008) for a square cavity with shear-free (○) and rigid (□) upper surfaces and a linear temperature profile compared with the asymptotic predictions $Z_0 = 2.10$ (— shear-free) and $Z_0 = 2.82$ (- - - rigid) of the present theory.

boundary-layer equations governing the plume flow. An approximate solution of this problem is used to provide an estimate of the core temperature, which is of order $R^{-1/15}$ in the shear-free case and order $R^{-2/65}$ in the rigid case. There appears to be no possibility that the core temperature is non-zero and finite as $R \to \infty$, because the cold end of the horizontal boundary layer is convectively dominated and in order that the circulation can be completed it follows that the temperature at the cold end of the upper surface is convected, via the vertical boundary layer, to the lower edge of the horizontal boundary layer. In that sense, the details of the vortex structure considered in § 5 are unimportant in terms of determining the core temperature in the cavity. The core temperature does depend, however, on the details of the horizontal boundary-layer flow through the parameter K associated with the velocity and temperature profiles near the cold end at the upper surface. Temperature profiles at the upper surface that generate higher values of K lead to higher core temperatures.

The main features of the asymptotic results can be compared with the results of Chiu-Webster *et al.* (2008). They carried out numerical computations of the full cavity flow for both shear-free and rigid upper surfaces with the linear temperature profile (3.17) for Rayleigh numbers up to $R = 10^{10}$. The streamlines and isotherms of the horizontal boundary-layer flow in figures 2 and 9 have the same features as those reported in the full numerical computations, including the characteristic region of horizontal flow reversal below the main two-way circulation near the top of the cavity. According to the present theory, the vortex centre is positioned at the cold end of the horizontal boundary layer at non-dimensional depth

$$z = R^{-1/5}Z_0 + \cdots, \quad R \to \infty, \tag{9.1}$$

where $Z_0 = 2.10$ in the shear-free case and $Z_0 = 2.82$ in the rigid case. This is compared with the numerical calculations of Chiu-Webster *et al.* (2008) for a square cavity ($A = 1$) in figure 12. In each case, the results are consistent with a gradual

approach to the asymptotic limit. The horizontal displacement of the vortex centre from the cold sidewall predicted by the asymptotic analysis is

$$x = R^{-2/9}\bar{\beta}_0^{1/6}\Theta_1^{-1/6}\xi_0 + R^{-4/15}\Theta_0^{-1/3}\Psi_0^{1/3}X_0 + \cdots, \quad R \to \infty. \tag{9.2}$$

Here the leading term is the displacement predicted by the approximate vortex solution of § 5 and the correction term represents the displacement of the vortex within the vertical boundary layer predicted in § 4. It is not clear that this is the leading correction, given that the vortex expansion itself may proceed in powers of $R^{-1/45}$. Inserting the values of X_0, ξ_0, $\bar{\beta}_0$, Θ_0, Ψ_0 and Θ_1 for the shear-free case gives

$$x = \{1.07R^{-2/9} + \cdots\} + \{3.15R^{-4/15} + \cdots\}, \quad R \to \infty. \tag{9.3}$$

For the rigid case, the corresponding result is

$$x = \{1.20R^{-2/9} + \cdots\} + \{3.20R^{-4/15} + \cdots\}, \quad R \to \infty. \tag{9.4}$$

The results (9.3) and (9.4) are compared with the numerical results of Chiu-Webster *et al.* (2008) for a square cavity in figure 13(*a*). The asymptotic predictions indicate the correct trend, and the fact that the entire corner region structure (regions III–V) involves terms of relative order $R^{-1/45}$ precludes the possibility of close agreement. This is also true of the maximum streamfunction value at the centre of the vortex. The theoretical prediction is

$$\psi = \{R^{11/45}\bar{\beta}_0^{7/6}\Theta_1^{-1/6}\Phi_0 + \cdots\} + \{R^{1/5}\Psi_0 + \cdots\}, \quad R \to \infty, \tag{9.5}$$

where the leading term is that predicted by the vortex analysis of § 5 and the correction allows for the underlying contribution from the horizontal boundary layer. Inserting the values of $\bar{\beta}_0$, Θ_1, Φ_0 and Ψ_0 for the shear-free case gives

$$\psi = 0.141R^{11/45} + 0.736R^{1/5} + \cdots, \quad R \to \infty \tag{9.6}$$

and for the rigid case

$$\psi = 0.130R^{11/45} + 0.560R^{1/5} + \cdots, \quad R \to \infty. \tag{9.7}$$

The results (9.6) and (9.7) are compared with the numerical results of Chiu-Webster *et al.* (2008) for a square cavity in figure 13(*b*). Remarkably, the asymptotic forms provide quite reasonable approximations over a large range of Rayleigh numbers. A slight divergence of the numerical and asymptotic results with increasing R is consistent with the existence of corrections to (9.6) and (9.7) that grow as $R \to \infty$, or with a reduction of less than 10 % in the value of Φ_0 in (5.16) predicted by the approximate vortex solution of § 5.

The Nusselt number predicted by the asymptotic theory is

$$Nu = R^{1/5}Nu_0 + \cdots, \quad R \to \infty, \tag{9.8}$$

with $Nu_0 = 0.27$ in the shear-free case and $Nu_0 = 0.17$ in the rigid case. This is in good agreement with the numerical results of Chiu-Webster *et al.* (2008) for a square cavity as shown in figure 14(*a*).

For a shear-free upper surface the core temperature predicted by the asymptotic form (7.14) is

$$T \sim 0.704R^{-1/15}, \quad R \to \infty \tag{9.9}$$

and for a rigid upper surface, the corresponding result, from (8.23), is

$$T \sim 0.364R^{-2/65}, \quad R \to \infty. \tag{9.10}$$

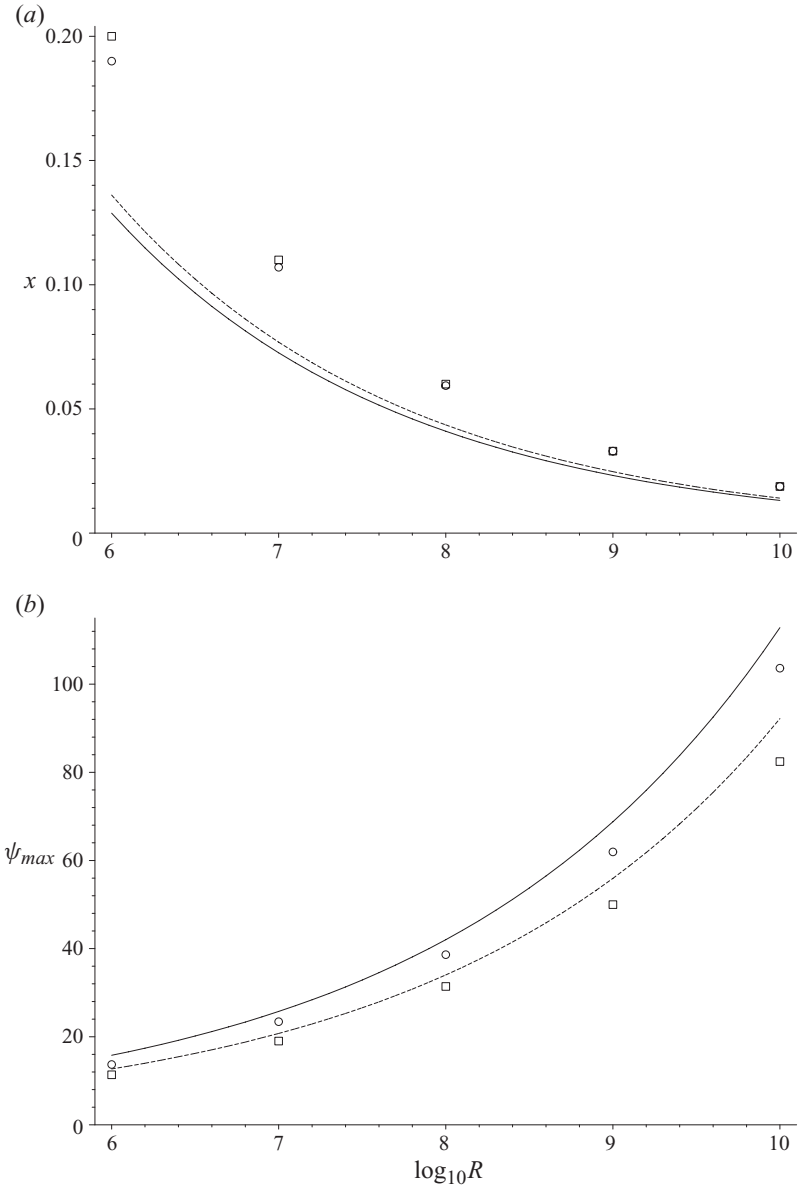

FIGURE 13. (*a*) The horizontal location of the vortex centre x and (*b*) the maximum streamfunction value ψ_{max} given by the computations of Chiu-Webster *et al.* (2008) for a square cavity with shear-free (○) and rigid (□) upper surfaces and a linear temperature profile compared with the asymptotic predictions (9.3) and (9.6) (— shear-free) and (9.4) and (9.7) (- - - rigid) of the present theory.

These are compared with the numerical results of Chiu-Webster *et al.* (2008) for a square cavity in figure 14(*b*). The asymptotic results rely on the values of $\tilde{T}_c$ predicted by the approximate solution of the plume problem, but are reasonably consistent with the numerical calculations.

Further work is needed to obtain accurate numerical solutions of the plume problem studied in § 7 and the vortex problem studied in § 5. Unfortunately, the scalings in the

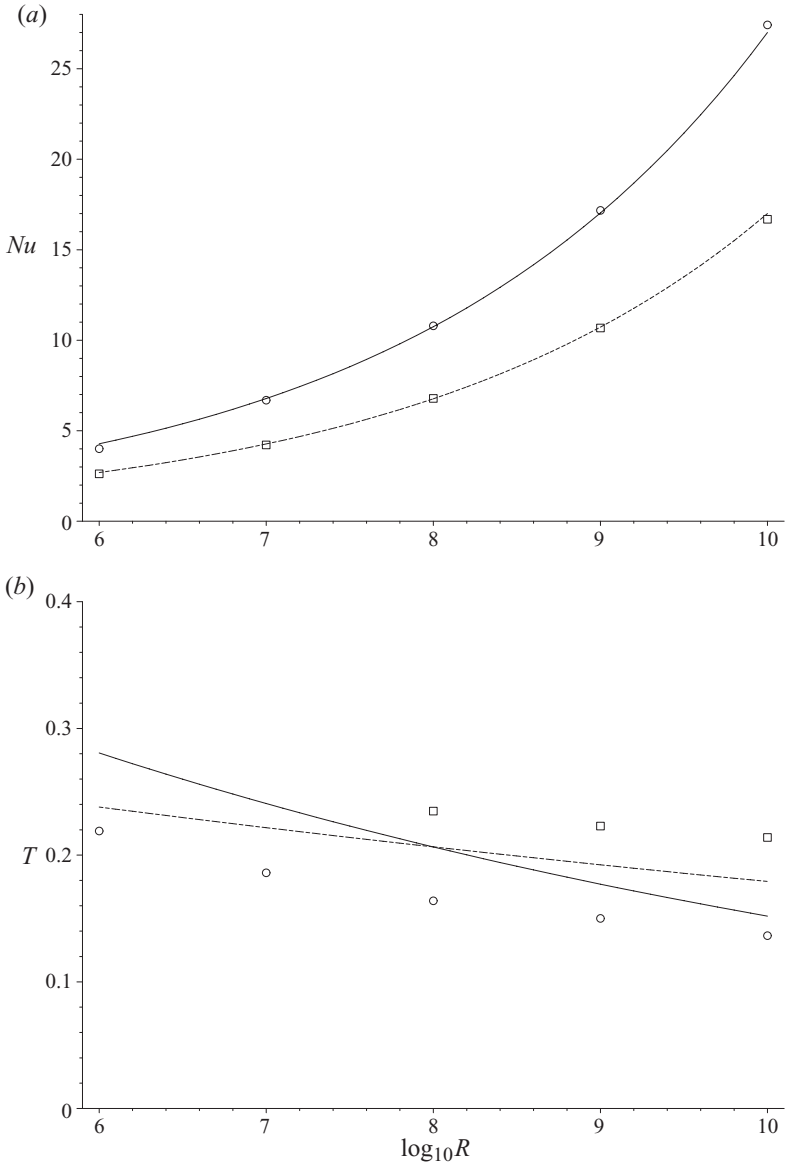

FIGURE 14. (*a*) The Nusselt number Nu and (*b*) the core temperature T given by the computations of Chiu-Webster *et al.* (2008) for a square cavity with shear-free (○) and rigid (□) upper surfaces and a linear temperature profile compared with the asymptotic predictions (9.8)–(9.10) of the present theory (— shear-free, - - - rigid).

Rayleigh number, especially in the upper cold corner, where regions of relative scale $R^{-1/45}$ are involved, means that the present asymptotic structure may not emerge in practice until the Rayleigh number is extremely large. An estimate of the validity of the horizontal structure can be made by comparing the depths of the two horizontal layers. For the main layer, the results of figures 2 and 9 suggest a typical scale $Z = 10$, giving $z \sim 10R^{-1/5}$. For the outer layer, the values $\tilde{Z}_0 = 0.841$ and 0.717 obtained in the shear-free and rigid cases suggest a typical scale $\tilde{Z} = 1$, corresponding to $z \sim R^{-2/15}$ in the shear-free case and $z \sim R^{-9/65}$ in the rigid case. This suggests

that the outer layer depth is large compared with the main layer depth provided that $R \gg 10^{15}$ in the shear-free case and $R \gg 10^{16.25}$ in the rigid case, values well beyond those of currently available numerical simulations. Despite this limitation, the asymptotic theory provides insight into the flow that adds to that gained from numerical simulations and with further investigation should help in understanding how the flow is modified at finite Prandtl numbers and in shallow geometries of relevance to ocean circulations and furnace-melt flows. For shallow geometries it seems likely that as $R \to \infty$ distinguished limits will arise when the depth of the cavity is comparable with that of either the outer horizontal layer or the main horizontal layer but further work is needed to confirm this and to investigate the details of the solution in each case.

The author is grateful for the helpful comments of three referees.

REFERENCES

Abramowitz, M. & Stegun, I. 1965 *Handbook of Mathematical Functions*. Dover.

Batchelor, G. K. 1954 Heat transfer by free convection across a closed cavity between vertical boundaries at different temperatures. *Quart. Appl. Math.* **12**, 209–233.

Batchelor, G. K. 1956 On steady laminar flow with closed streamlines at large Reynolds number. *J. Fluid Mech.* **1**, 177–190.

Chiu-Webster, S., Hinch, E. J. & Lister, J. R. 2008 Very viscous horizontal convection. *J. Fluid Mech.* **611**, 395–426.

Daniels, P. G. & Punpocha, M. 2005 On the boundary-layer structure of cavity flow in a porous medium driven by differential heating. *J. Fluid Mech.* **532**, 321–344.

Gramberg, H. J. J., Howell, P. D. & Ockenden, J. R. 2007 Convection by a horizontal thermal gradient. *J. Fluid Mech.* **586**, 41–57.

Hughes, G. O., Griffiths, R. W., Mullarney, J. C. & Peterson, W. H. 2007 A theoretical model for horizontal convection at high Rayleigh number. *J. Fluid Mech.* **581**, 251–276.

Killworth, P. D. & Manins, P. C. 1980 A model of confined thermal convection driven by non-uniform heating from below. *J. Fluid Mech.* **98**, 587–607.

Krause, D. & Loch, H. (Eds) 2002 *Mathematical Simulation in Glass Technology*. Springer.

Mullarney, J. C., Griffiths, R. W. & Hughes, G. O. 2004 Convection driven by differential heating at a horizontal boundary. *J. Fluid Mech.* **516**, 181–209.

Rossby, T. 1965 On thermal convection driven by non-uniform heating from below: an experimental study. *Deep Sea Res.* **12**, 9–16.

Rossby, T. 1998 Numerical experiments with a fluid heated non-uniformly from below. *Tellus* **50A**, 242–257.

Siggers, J. H., Kerswell, R. R. & Balmforth, N. J. 2004 Bounds on horizontal convection. *J. Fluid Mech.* **517**, 55–70.

Stern, M. E. 1975 *Ocean Circulation Physics*. Academic Press.

Stommel, H. 1962 On the smallness of the sinking regions in the ocean. *Proc. Natl Acad. Sci.* **48**, 766–772.

Wang, W. & Huang, R. X. 2005 An experimental study on thermal circulation driven by horizontal differential heating. *J. Fluid Mech.* **540**, 49–73.